ARPHA Preprints

PENSOFT

PREPRINT

Author-formatted, not peer-reviewed document posted on 03/09/2026

DOI: https://doi.org/10.3897/arphapreprints.e214223

Chronology and emplacement dynamics of the Poschiavo rock avalanche at the Younger Dryas–Holocene transition

Janine Fankhauser, David Mair, Susan Ivy-Ochs, Jordan Aaron, Marcus Christl, Philip Gautschi, Naki Akçar

ARPHA Preprints *Author-formatted, not peer-reviewed document posted on 03/09/2026.* DOI: https://doi.org/10.3897/arphapreprints.e214223

Chronology and emplacement dynamics of the Poschiavo rock avalanche at the Younger Dryas–Holocene transition

Janine Fankhauser[1], David Mair[1], Susan Ivy-Ochs[2,3], Jordan Aaron[3], Marcus Christl[2], Philip Gautschi[2], Naki Akçar[1]

[1] *Institute of Geological Sciences, University of Bern*

[2] *Laboratory of Ion Beam Physics, ETH Zurich*

[3] *Department of Earth and Planetary Sciences, ETH Zurich*

Abstract

The Mota dal Meschin deposit in the Poschiavo Valley, southeastern Switzerland, has previously been interpreted as glacial or mass-movement material, and its age, source area, and relationship to Lake Poschiavo have remained uncertain. In this study, we combine geomorphological mapping, sedimentological and petrographic observations, surface exposure dating with cosmogenic ^{10}Be measurements, palaeotopographic reconstruction, volume estimation, and rock avalanche runout modelling with DAN3D® to investigate the origin and emplacement of the deposit. Its irregular morphology, abundance of large angular boulders, locally preserved openwork fabric, and absence of a continuous overlying till support a rock avalanche origin and provide no evidence for substantial post-emplacement glacier overriding. Nine ^{10}Be exposure ages define a statistically coherent population with a mean age of 11.1 ± 0.5 ka, indicating that the preserved surface deposit and Garbella ridge formed during one Early Holocene event, shortly after the Younger Dryas-Holocene transition. However, this chronology does not exclude smaller or buried secondary failures. Petrographic, topographic, and modelling evidence favours a source area for the material on the southwestern valley flank between Giümelin and Corn dal Solcun. The preserved deposit volume is estimated at approximately 94 Mm^3, corresponding to an intact source volume of about 79 Mm^3 assuming 20% bulking. The isolated deposits at Mota dal Meschin, La Motina, and Li Plani are interpreted as remnants of a formerly more continuous deposit subsequently modified by river incision and fan deposition. The rock avalanche probably contributed to obstruction of the Poschiavino Valley and the evolution of Lake Poschiavo. Earlier glaciations likely preconditioned the source slope, whereas the immediate climatic, hydrological, or seismic trigger remains unresolved.

Keywords

Alpine mass movements, ^{10}Be surface exposure dating, Younger Dryas – Holocene transition, Rock avalanche, Runout modelling, Swiss Alps

Introduction

Glacial erosion and catastrophic rock-slope failures are among the principal processes shaping high-relief valleys in the European Alps (Grämiger et al. 2017; Ivy-Ochs et al. 2017; Reynard et al. 2021). Large rock avalanches (>10^6 m^3) can rapidly modify valley morphology, redistribute large volumes of sediment, and profoundly influence subsequent landscape evolution (Abele 1974; Prager et al. 2008; McColl 2012; Ivy-Ochs et al. 2009a; Grämiger et al. 2016). Although numerous large rock avalanches occurred in the Swiss Alps following the Last Glacial Maximum (LGM; Ivy-Ochs et al. 2022), their timing does not show a simple relationship with glacier retreat (Prager et al. 2008; McColl 2012). Some failures occurred during or shortly after deglaciation, whereas others followed several millennia later, indicating that glacial erosion, debuttressing, and stress redistribution commonly precondition slopes, while progressive rock-mass weakening and short-lived external perturbations may ultimately trigger collapses (Prager et al. 2008; McColl 2012; Ballantyne et al. 2014; Grämiger et al. 2017).

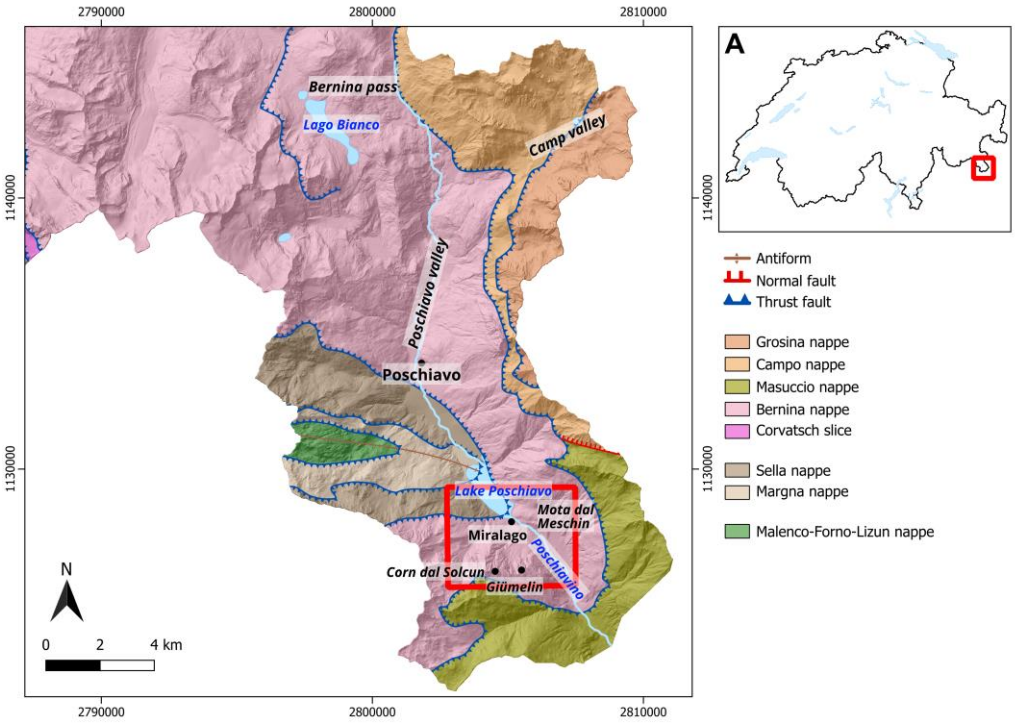

Figure 1. Tectonic map of the south eastern part of Switzerland TK500 ©Federal Office of Topography Swisstopo 2024). Inset **A** illustrates the position of the study site.

Rock-slope failure generally results from the progressive interaction of geological, glacial, thermal, and hydrological processes rather than from a single environmental change (McColl 2012; Krautblatter et al. 2013; Grämiger et al. 2017). The glacial periods in the Quarternary progressively deepened Alpine valleys and steepened adjacent valley flanks, producing high-relief glacial troughs and overdeepened basins (Preusser et al. 2010; Leith et al. 2014a; Schlüchter et al. 2021; Seguinot and Delaney 2021). Repeated cycles of glacier loading and unloading, together with progressive

valley incision, altered the near-surface stress field and promoted microcrack development and fracture propagation within the surrounding rock mass (Leith et al. 2014a, 2014b; Grämiger et al. 2017). Glacier retreat may therefore have reduced lateral support and contributed to paraglacial slope instability, leading to rock failures shortly after the ice retreat (e.g., Hartmeyer et al. 2020). However, it is more appropriately regarded as a preconditioning or preparatory process than as a direct failure trigger, particularly where collapse occurs centuries or millennia after deglaciation (McColl 2012; Ballantyne et al. 2014; Grämiger et al. 2017). At higher elevations, permafrost degradation can further reduce the strength of ice-filled discontinuities and promote progressive rock-mass destabilization (Krautblatter et al. 2013; Patton et al. 2021). Once a critically unstable state is reached, final failure may be initiated by short-lived perturbations such as seismic shaking, pore-water-pressure increases caused by intense precipitation or snowmelt, or temperature-induced stress changes (Keefer 1984; Gischig et al. 2011a, b; Nie et al. 2017; Fan et al. 2019). However, because such transient forcing is rarely preserved in the geological record, the immediate trigger of prehistoric rock avalanches commonly remains uncertain (McColl 2012; Grämiger et al. 2016).

The deposits and chronologies of large prehistoric rock avalanches provide long-term records of Alpine slope instability beyond the relatively short historical and instrumental record and therefore complement observations of currently deforming rock slopes (Prager et al. 2008; Breitenmoser et al. 2022; Manconi et al. 2024). Establishing their chronology, volume, source geometry, and emplacement dynamics, together with the geological and geomorphological context of the failed slopes, is essential for identifying possible temporal clustering and evaluating the relative contributions of glacial preconditioning, climatic variability, and seismic forcing (Prager et al. 2008; Grämiger et al. 2016; Singeisen et al. 2020; Pfiffner et al. 2023). Several dated Alpine rock avalanches occurred during the Lateglacial and Early Holocene, such as the Lurnigalp, Klein Rinderhorn and Daubensee events (Grämiger et al. 2016; Bucher et al. 2024). However, the apparent temporal concentration of these failures should not be interpreted as evidence for a common trigger, because individual slopes differ in lithology, structure, glacial history, and progressive damage, and because uncertainties in both event inventories and age determinations remain substantial (Prager et al. 2008; McColl 2012; Jacquemart et al. 2024).

Reconstructing long-term records of rock-slope failure is challenging because prehistoric rock avalanche deposits may be reworked, buried, or fragmented by subsequent glacial, fluvial, and periglacial processes (Shugar and Clague 2011; Cook et al. 2013; Schleier et al. 2015; Bucher et al. 2024). In formerly glaciated valleys, poorly sorted bouldery rock avalanche deposits may resemble till or other glaciogenic landforms, leading to ambiguous or erroneous genetic interpretations (Porter and Orombelli 1980; Akçar et al. 2012; Cook et al. 2013; Schleier et al. 2015; Bucher et al. 2024). These preservation and classification problems can produce incomplete inventories and obscure the spatial and temporal distribution of large slope failures. Together with the rarity of such events and the limited duration of observational

records, this restricts our ability to identify temporal trends and evaluate relationships with climatic change, particularly for large rock avalanches (Prager et al. 2008; Jacquemart et al. 2024). This limitation is particularly relevant in the European Alps, where pronounced warming, shifts in precipitation patterns and intensity, and widespread reductions in snow cover are altering the environmental conditions and affect the high-mountain slope stability (Kotlarski et al. 2023). Such uncertainties are best addressed through an integrated approach combining detailed geomorphological and geological mapping, sedimentological and petrographic observations, direct geochronology, reconstruction of pre-failure topography, and numerical runout modelling (Singeisen et al. 2020; Bucher et al. 2024; Rubin et al. 2026). The resulting insights are particularly important for hazard and risk assessment in the Alps.

The Mota dal Meschin deposit at the southern end of Lake Poschiavo exemplifies these interpretive difficulties (Figure 1 and 2). Its origin and stratigraphic relationship with the surrounding glacial and fluvial deposits remain unresolved. Earlier mapping and subsequent studies have yielded contrasting interpretations of the bouldery succession and its relationship to glacial deposits (Figure 3) (Staub 1946; Burga 1987; Zwahlen 2019; ©Federal Office of Topography Swisstopo 2026). Based on boreholes near Miralago, Zwahlen (2019) interpreted the succession as recording a main Younger Dryas rock avalanche event followed by secondary failures, with tills occurring below, between, and above the rock avalanche material; radiocarbon-dated wood fragments provided chronological control on the succession. In contrast, regional glacial and vegetation reconstructions suggest that the main Poschiavo Valley near Miralago may already have been ice-free before the Younger Dryas (Burga 1987). Consequently, it remains uncertain whether the Mota dal Meschin formed during a single catastrophic failure or through several events, whether glacier ice was present during or after emplacement, and how the deposit relates to the present morphology and development of Lake Poschiavo.

In this study, we investigate the origin, chronology, and emplacement dynamics of the Mota dal Meschin bouldery deposit at 1156 m a.s.l. at the southern end of Lake Poschiavo, southeastern Switzerland (Figures 1 and 2). We test the hypothesis that the deposit and associated remnants formed during a single large rock avalanche event originating from the southwestern valley flank. To evaluate this hypothesis, we combine detailed geomorphological mapping and boulder inventories, petrographic comparison of deposit and source lithologies, surface exposure dating with cosmogenic ^{10}Be, reconstruction of the pre-failure topography, volume estimation, and numerical runout modelling with DAN3D® (Hungr and McDougall 2009). Specifically, we assess whether the mapped deposits share a common origin and age, identify the most plausible source area, reconstruct the magnitude and mobility of the failed rock mass, and evaluate whether glacier ice influenced its emplacement. Our results indicate that the deposits were emplaced during a single rock avalanche at the Younger Dryas–Holocene transition, when the main Poschiavo valley was probably ice-free.

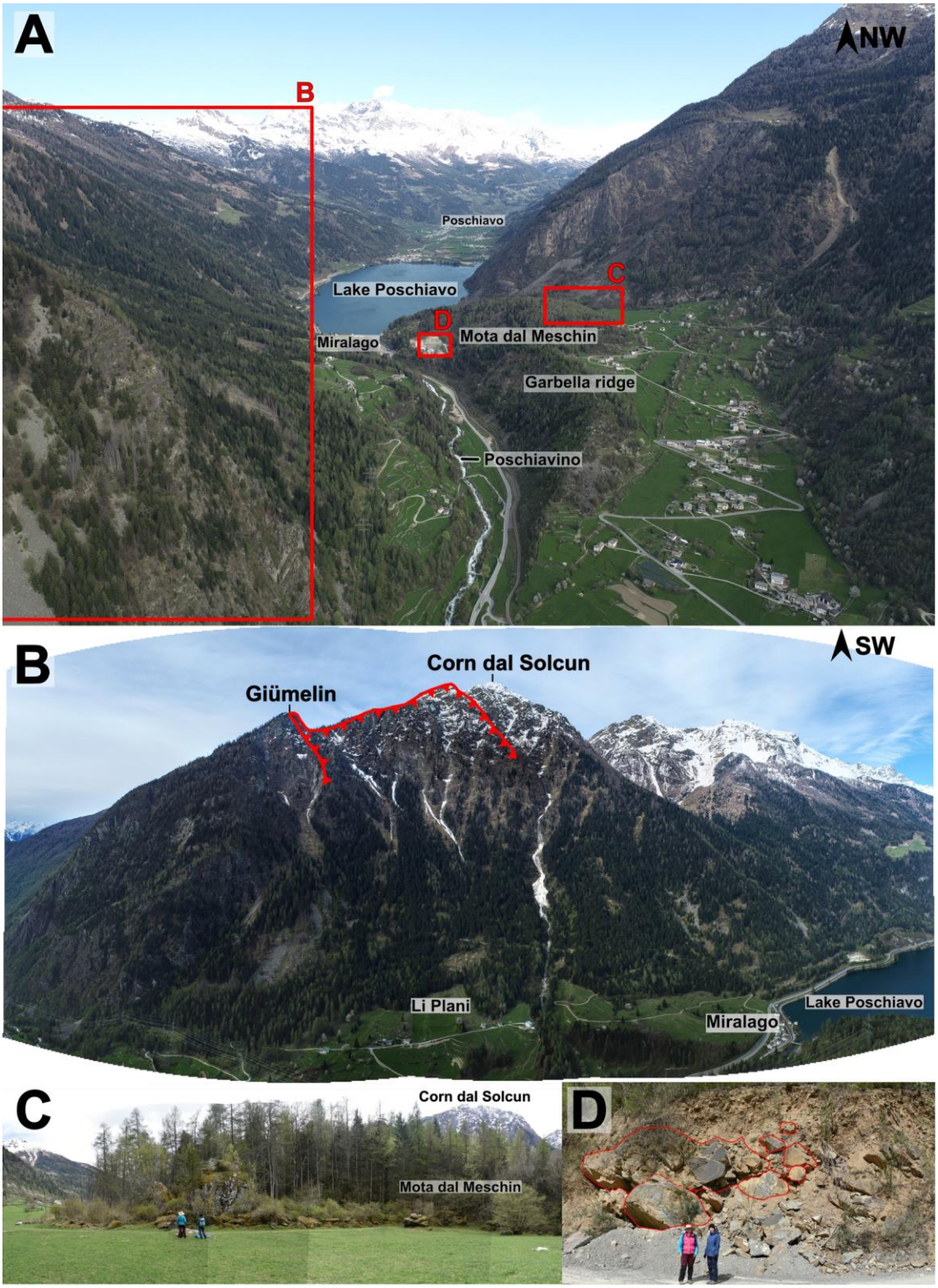

147

148 **Figure 2. A** Aerial image of the Study area, view upvalley towards northwest; **B** Aerial
149 image of the the release area, captured from the top of the Mota dal Meschin. The red
150 line indicates the release scarp; **C** Panoramic view from north of the Mota dal Meschin
151 towards the south; **D** Outcrop from the gravel pit Mota di Miralago. Some larger
152 boulders are outlined in red.

Study Area and previous studies

The Poschiavo valley is located in southeastern Switzerland, in the Canton of Graubünden, close to the Italian border (Figure 1). The valley has a NW – SE orientation and is around 25 km long and up to 10 km wide. It is drained southward by the Poschiavino River and contains the Lake Poschiavo between Le Prese and Miralago. Miralago is located at 965 m a.s.l., which is just slightly higher than the lake surface at 961.7 m a.s.l. The valley floor is generally narrow, flat and has a sharp transition to the steep hillslopes of the surrounding mountains, which are all between 2000 m a.s.l. and 3000 m a.s.l. high. The study area is around 9.1 km^2 large, whereas the rock avalanche deposits combine to a total of 1.6 km^2. The study area spans around 4 km NE – SW and 2.5 km NW – SE and encompasses the southern lake basin, the prominent Mota dal Meschin landform at approximately 1156 m a.s.l., and the adjacent valley flanks (Figures 1 and 2). The tentative release area investigated in this study lies between Giümelin (2040 m a.s.l.) and Corn dal Solcun (2513 m a.s.l.), at elevations of approximately 1800–2350 m a.s.l. (Figure 2).

The study area lies close to the tectonic boundary between units of the upper Penninic, Salassic and Austroalpine domains (Figure 1). The Sella Nappe, assigned to the Salassic domain, consists predominantly of upper-crustal granitoids and paragneisses and is structurally overlain by units of the Austroalpine nappe stack, including the basement-dominated Bernina Nappe Complex (Gouffon 2024). The Bernina basement is dominated by Late- to post-Variscan magmatic rocks intruding an older metamorphic basement, whereas the Campo Nappe Complex, exposed regionally east of Lake Poschiavo, consists predominantly of Variscan metasedimentary basement with subordinate magmatic rocks (Gouffon 2024).

During the LGM, the Poschiavo Valley was occupied by a glacier connected to the regional Alpine ice network (Bini et al. 2009). Subsequent deglaciation was interrupted by several Alpine Lateglacial glacier readvances. The Gschnitz Stadial occurred at approximately 17–16 ka, before the onset of the Bølling warm interval, whereas the younger Egesen advances broadly correspond to the Younger Dryas (Ivy-Ochs et al. 2006, 2023a, 2023b). Burga (1987) reconstructed the regional glacier and vegetation history of the southern Rhaetian Alps and inferred the main Poschiavo Valley near Miralago as having become ice-free before the Younger Dryas. Such a configuration would be compatible with Younger Dryas glacier readvances restricted to higher tributary catchments rather than a renewed occupation of the main valley at Miralago (Burga 1987).

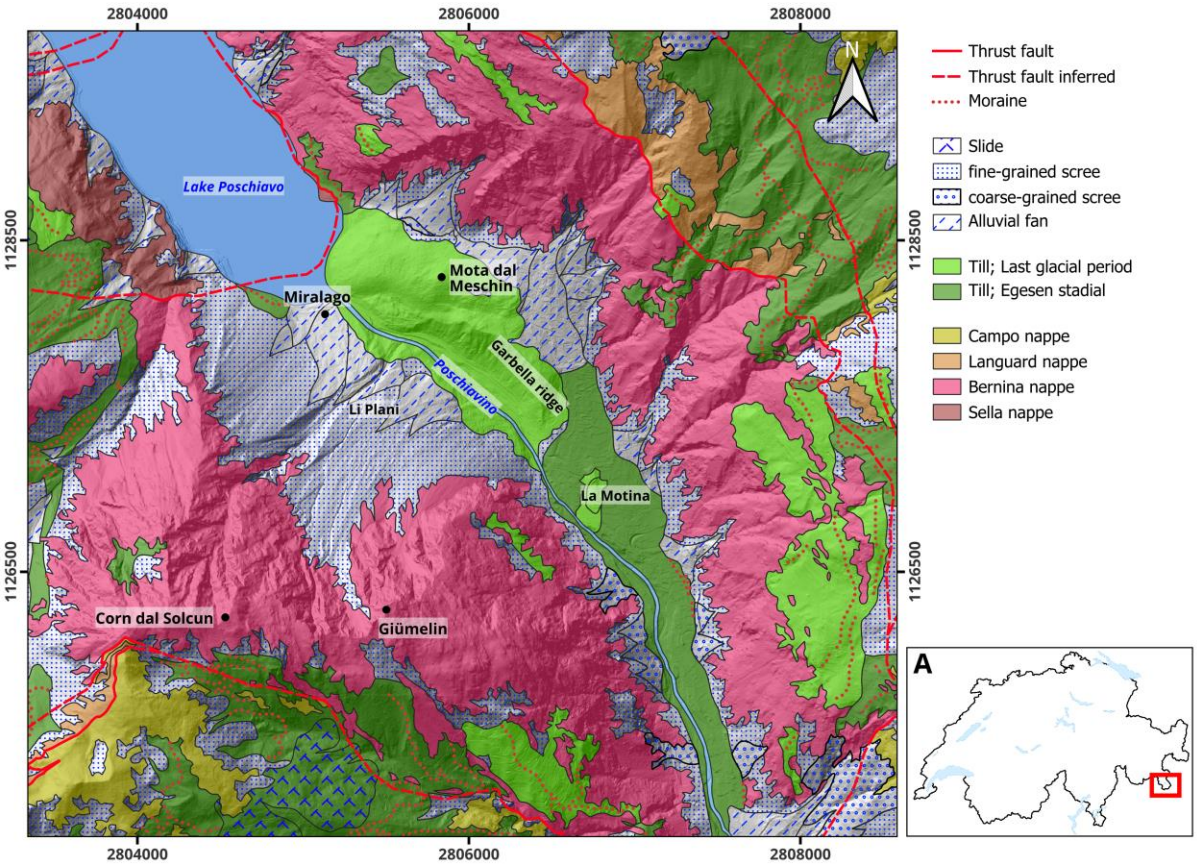

Figure 3. Geological overview map of the study region (adapted after the Geocover Mapsheet LK1298 1:25'000 ©Federal Office of Topography Swisstopo 2026). Inset **A** illustrates the position of the study site.

Staub (1946) produced the first detailed geological mapping of the lower Poschiavo Valley and distinguished several glacial and mass-movement units, including deposits assigned to the Veltliner (pre-Younger Dryas, 14.7 ka BP; Zwahlen 2019) and Brusasker stages (Younger Dryas; Staub 1946). Geological and geotechnical investigations associated with the proposed Lago Bianco pumped-storage project subsequently provided borehole information from the Miralago area. Based on the stratigraphic succession and radiocarbon-dated wood fragments (ca. 12.0 ± 0.2 cal kyr BP), Zwahlen (2019) interpreted a principal rock avalanche event during the Younger Dryas, followed by several secondary failures no later than the Early Holocene, or Preboreal. Furthermore, the study identified till units below, between and above the interpreted rock avalanche deposits and proposed that the resulting succession ultimately dammed the Poschiavino River and formed Lake Poschiavo. Zwahlen (2019) attributed the underlying till to the Veltliner Stage of Staub (1946), tentatively placing them near the Oldest Dryas–Bølling transition, and the intercalated and overlying till to the multiphase Brusasker Stage, which would be correlated broadly with the Younger Dryas. The study explicitly cautioned that neither local stage could be correlated with the Gschnitz Stadial (cf. Ivy-Ochs et al. 2023a). These contrasting interpretations raise several unresolved questions, which we address in this study: whether the Mota dal Meschin deposit formed during a single catastrophic event or

through several successive failures, whether glacier ice was present during or after emplacement, and what role the rock avalanche played in damming the Poschiavino River and forming Lake Poschiavo.

Methods

Mapping and petrographic analysis

The mapping of the surface geology and geomorphology of the Mota dal Meschin area was based on field observations, remote sensing, and the 0.5 m resolution swissAlti3D® digital elevation model (DEM; ©Federal Office of Topography Swisstopo 2023). All spatial data were compiled and analysed in QGIS® version 3.40. Mapping was conducted at a scale of 1:10,000. The mapped surface units comprised bedrock, rock avalanche deposits, scree, debris-flow fans, alluvial fans and polygenetic cones. Additional geomorphological features included large boulders, levees, erosional scarps, anthropogenic modifications, and the release scarp. The classification of geomorphological units was adapted from the approaches of Bucher et al. (2024) and Rubin et al. (2026). Tectonic contacts, thrust faults, and the regional subdivision of the crystalline bedrock were compiled from the Geocover dataset (map sheet LK1298; ©Federal Office of Topography Swisstopo 2026, 1:25'000) and the tectonic map of Switzerland 1:500’000 (©Federal Office of Topography Swisstopo 2024).

During fieldwork, boulders exceeding 1.5 m in height were included in an inventory. Their positions were recorded using a handheld GNSS receiver (Garmin Oregon 550t) with an accuracy of less than 10 m. The position and altitude of the boulders was then cross-checked using the 0.5 m resolution swissAlti3D® digital elevation model (DEM; ©Federal Office of Topography Swisstopo 2023). The boulder lithology and macroscopic fabric were described to evaluate spatial variations within the deposit and their compatibility with potential source rocks. Based on field observations, the boulders were provisionally divided into two groups: (1) massive granitoid to weakly foliated gneiss and (2) strongly foliated or schistose gneiss, characterized by foliation spacing of less than 5 cm. To extend the mapping into steep or inaccessible terrain, Aerial imagery acquired with DJI Phantom 4 Pro and DJI Mavic 3 uncrewed aerial vehicles was used. This was done to support qualitative interpretation of geomorphic features, and to cross-check the field mapping.

Representative boulder samples were collected across Mota dal Meschin from both field-defined lithological groups. The boulders were sampled randomly across Mota dal Meschin with special regards to cover both above-described categories of boulders. Reference samples were additionally collected from bedrock outcrops on the northeastern and southwestern valley flanks. Petrographic thin sections were examined using transmitted-light microscopy under plane- and cross-polarised light. Mineral assemblages, grain-scale textures, and the presence and intensity of micro-foliation were documented. These observations were compared with the macroscopic boulder classification, the reference bedrock samples, and published descriptions of the regional crystalline rocks (Spillmann 1993; Gouffon 2024) to evaluate the

compatibility of the boulder lithologies with potential source areas. The mineralogical composition, in combination with the macroscopic rock fabric/texture, allowed us to confirm the preliminary lithological classification during fieldwork, and to identify the potential source area.

Surface exposure dating with cosmogenic ^{10}Be

To determine the emplacement age of the Mota dal Meschin deposit and test whether the main deposit and the southeastern Garbella ridge formed contemporaneously, we collected 11 samples from granite and gneiss boulders in April 2024. Eight samples were collected from the main Mota dal Meschin deposit and three from the Garbella ridge southeast of it. Sampling followed established strategies for surface exposure dating (Akçar et al. 2011). We selected large, stable boulders that protruded above the surrounding ground surface and showed no visible evidence of toppling, exhumation, spalling or post-depositional displacement (Heyman et al. 2016). Vegetated or persistently shielded surfaces were avoided. Samples were removed from the upper boulder surfaces using a diamond-blade angle grinder, hammer and chisel. For each sample, we recorded its location, altitude, boulder dimensions, sample thickness, surface orientation and topographic shielding. Sampled boulders ranged from 0.9 to 4.3 m in protruding height, sample thicknesses ranged from 3 to 5 cm, and sample elevations ranged from 1097 to 1155 m a.s.l. (Table 1).

Table 1. Sample information of the boulders from the Poschiavo Valley.

Sample name	Altitude (m a.s.l.)	Latitude, °N (DD.DD) WGS84	Longitude, °E (DD.DD) WGS84	Boulder height (m)	Sample thickness (cm)	Shielding correction factor
POSC-1	1097.7	46.27155	10.11213	1.8	5.0	0.96191
POSC-2	1097.7	46.27155	10.11213	3.8	3.0	0.96191
POSC-3	1097.7	46.27155	10.11213	4.3	4.5	0.96191
POSC-4	1152.3	46.27422	10.10919	1.7	5.0	0.95405
POSC-5	1152.3	46.27422	10.10919	1.8	4.0	0.95405
POSC-6	1155.0	46.27436	10.10956	0.9	3.5	0.95405
POSC-7	1138.0	46.2743	10.11152	1.7	5.0	0.95402
POSC-8	1137.8	46.27442	10.11149	2.4	5.0	0.95402
POSC-9	1147.8	46.27465	10.11003	2.4	5.0	0.94319
POSC-10	1140.4	46.27384	10.11278	2.0	4.0	0.95449
POSC-11	1138.4	46.27373	10.11305	1.6	5.0	0.95449

Processing of eleven samples for ^{10}Be extraction was undertaken at the Surface Exposure Dating Laboratory of the University of Bern. Lichen was removed before the samples were crushed and sieved to a grain size fraction of 250–400 µm. Magnetic

minerals were removed, and quartz was isolated and purified following the procedures of Akçar et al. (2017), based on Kohl and Nishiizumi (1992). Cosmogenic ^{10}Be was extracted following Akçar et al. (2012). For nine samples, approximately 35 g of purified quartz were dissolved after addition of ca. 0.25 mg of ^{9}Be from carrier solution (Table 2). Due to laboratory capacity constraints, samples POSC-9 and POSC-10 were not processed beyond quartz purification.

The ^{10}Be/^{9}Be ratios were measured at the MILEA system at the ETH Zurich AMS facility (Maxeiner et al. 2019). The measured ratios were normalized to the ETH in-house standards S2007N and S2010N (Christl et al. 2013), assuming a ^{10}Be half-life of 1.39 Ma (Chmeleff et al. 2010; Korschinek et al. 2010). The ^{10}Be/^{9}Be isotopes were corrected by subtracting a long-term full-process blank ratio of (2.90 ± 0.25) x 10^{-15}, which represents a weighted averaged mean of 35 full-process blank-ratios measured from the same carrier bottle, from each measured isotope ratio. This amounted to blank corrections between 1.2% and 1.3% for the respective samples.

Surface exposure ages were calculated using version 3 of the online exposure-age calculator described by Balco et al. (2008), formerly known as the CRONUS-Earth online calculator. Production rates were scaled for latitude and altitude using the time-dependent Lal (1991) and Stone (2000) scaling scheme (Lm) that uses a magnetic field reconstruction based on Lifton (2016). The calculations accounted for sample thickness using an attenuation length of 160 g/cm^{-2}, topographic shielding following Dunne et al. (1999), a rock-surface erosion rate of 1 mm/ka^{-1} (André 2002), and a rock density of 2.65 g/cm^{-3}. Topographic-shielding correction factors were calculated following Tikhomirov et al. (2014). The sample-specific input parameters are provided in Table 1. No correction for snow cover was applied. The sampled boulders were large, protruded prominently above the surrounding deposit surface, and were therefore assumed to experience limited persistent snow accumulation and frequent wind removal of snow (Gosse and Phillips 2001; Heyman et al. 2016; Ye et al. 2023). The exposure-age dataset was additionally evaluated using the Probabilistic Cosmogenic Age Analysis Tool, P-CAAT, in MATLAB (Dortch et al. 2022). P-CAAT was used to identify potential statistical outliers and generate probability-density distributions of the ^{10}Be exposure ages.

Pre-failure surface reconstruction, volume estimation, and runout modelling

To reconstruct the pre-failure landscape and estimate the volume of the Poschiavo rock avalanche, we combined the present-day digital elevation model, mapping, lake-bathymetric information, and borehole and geological-profile data from Zwahlen (2019). Boreholes that reached bedrock were used as fixed elevation constraints for reconstructing the basal surface beneath the rock avalanche deposit, whereas boreholes that did not reach bedrock provided minimum-depth constraints. The reconstruction encompassed the source area, the runout corridor, the present lake basin and the mapped depositional area.

Contour lines with a vertical interval of 10 m were extracted from the present-day DEM raster and manually modified in QGIS to approximate the pre-event topography. We reconstructed the pre-event topography by assuming a uniform U-shaped valley. We checked the deposit thickness and valley shape by creating multiple cross sections in NE – SW and NW – SE orientation over the rock avalanche deposits and release area. The full extent of the rock avalanche deposit was interpolated based on the three different sediment bodies identified in the field, and for the volume calculations we ignored any recent deposits such as polygenetic cones that are overlying the rock avalanche. In the deposition area, the reconstructed contours were constrained by the present lake depth, borehole information and the geological cross-sections of Zwahlen (2019). In the source area, the pre-failure slope was reconstructed from the geometry of the adjacent unaffected slopes, the mapped boundaries of the release area and the required source volume. The edited contours were interpolated using the GRASS GIS (Neteler et al. 2012) tools v.in.ogr.gqis, v.to.rast.attr and r.surf.contour in QGIS to produce a DEM with a grid resolution of 10 x 10 m (McDougall 2017). The reconstructed surface was subsequently smoothed using the SAGA Smoothing (Vigra) tool (Conrad 2009). to remove interpolation artefacts while retaining the principal valley and slope geometry for further usage of the DEM in the DAN3D® program (McDougall and Hungr 2004).

Deposit thickness was calculated from the elevation difference between the reconstructed basal surface and the present-day surface using the raster calculator in QGIS (Grämiger et al 2016). The deposit volume was obtained by integrating the positive elevation differences across the mapped depositional area. The pre-failure source topography was reconstructed iteratively so that the corresponding source volume was compatible with the deposit-volume estimate after accounting for fragmentation and bulking. We assumed that fragmentation increased the volume of the failed rock mass by 20%. This increase corresponds to typical changes in porosity values for rock avalanche deposits (Hungr and Evans 2004). The reconstructed pre-failure surface formed the basis of the DAN3D® path-topography input, whereas the thickness and spatial distribution of the initial source mass were calculated from the difference between the reconstructed pre-failure and post-failure surfaces in the release area. Due to limited borehole information and unknown amount of erosion since deposition, we assume an uncertainty of around 20% for the volume calculation.

Runout was back-analysed using DAN3D®, a depth-averaged Lagrangian model that simulates rapid mass movement over three-dimensional terrain using a smoothed-particle hydrodynamics formulation (McDougall and Hungr 2004; McDougall, 2017). The model requires the path topography, the initial thickness and distribution of the source mass, the selected basal rheology, and material parameters describing the moving mass and underlying path. We applied the Voellmy rheology, in which basal resistance is controlled principally by the dimensionless friction coefficient μ and turbulence coefficient ξ. The internal friction angle and unit weight of the moving mass were specified independently.

Two configurations were evaluated. In the uniform-material configuration, a single set of basal parameters was assigned to the entire runout path. In the spatially variable configuration, the path was divided into bedrock and valley-floor sediment zones, and separate friction coefficients μ were assigned to these materials. The internal friction angle and unit weight were held constant at 30° and 20 kNm^{-3} for both configurations.

The model parameters were calibrated by comparing the simulated runout with the mapped distribution of the rock avalanche deposits. Model performance was evaluated from agreement with the distal and lateral deposit limits, the distribution of material around Mota dal Meschin and the distal remnants, and the reconstructed deposit-thickness pattern. The preferred parameter sets were those that reproduced these observations while minimizing simulated deposition outside the mapped rock avalanche area. Modelled flow velocities, travel times and final deposit thicknesses were extracted from the preferred uniform and spatially variable simulations.

Results

Surficial Geology

The mapped area extends from the southern end of Lake Poschiavo into the lower Poschiavo Valley and includes crystalline bedrock, slope deposits, fluvial landforms, and three spatially separated bodies classified as rock avalanche deposits (Figure 4). Granite and gneiss crop out extensively along both valley flanks. Discontinuous scree aprons occur at the base of the steeper bedrock slopes, while polygenetic cones cover large parts of the southwestern valley flank and smaller areas north and northeast of the main deposit. A large debris-flow fan occupies much of the eastern valley floor, and smaller alluvial fans occur at the outlets of tributary channels. Numerous levees and erosional channels are preserved on the polygenetic cones and debris-flow deposits. The Poschiavino River drains southward from Lake Poschiavo and follows the southern to southeastern margin of the main bouldery deposit.

The largest mapped rock avalanche body forms the Mota dal Meschin landform immediately south of Lake Poschiavo (Figure 4). It consists of a broad, elevated northwestern sector adjacent to the lake and a narrower ridge-like extension toward the southeast. This main deposit is covering an area of around 1 km^2, measures between 750 – 830 m at the widest part and is approximately 1930 m long. It reaches a maximum elevation of approximately 1157 m a.s.l. at the top of Mota dal Meschin and has an irregular surface that is markedly rougher than the surrounding alluvial and debris-flow surfaces. Several erosional scarps occur along its southern and southeastern margins and locally within the deposit. The erosional scarps closer to the lake lie mostly around altitudes between 980 – 1025 m a.s.l. The erosional scarps further downstream are located at lower altitudes and go as low as 770 m a.s.l. The boreholes KB25 and KB27 of Zwahlen (2019) are located close to the northern margin of the main deposit, where the deposit is bordered or incised by the Poschiavino River.

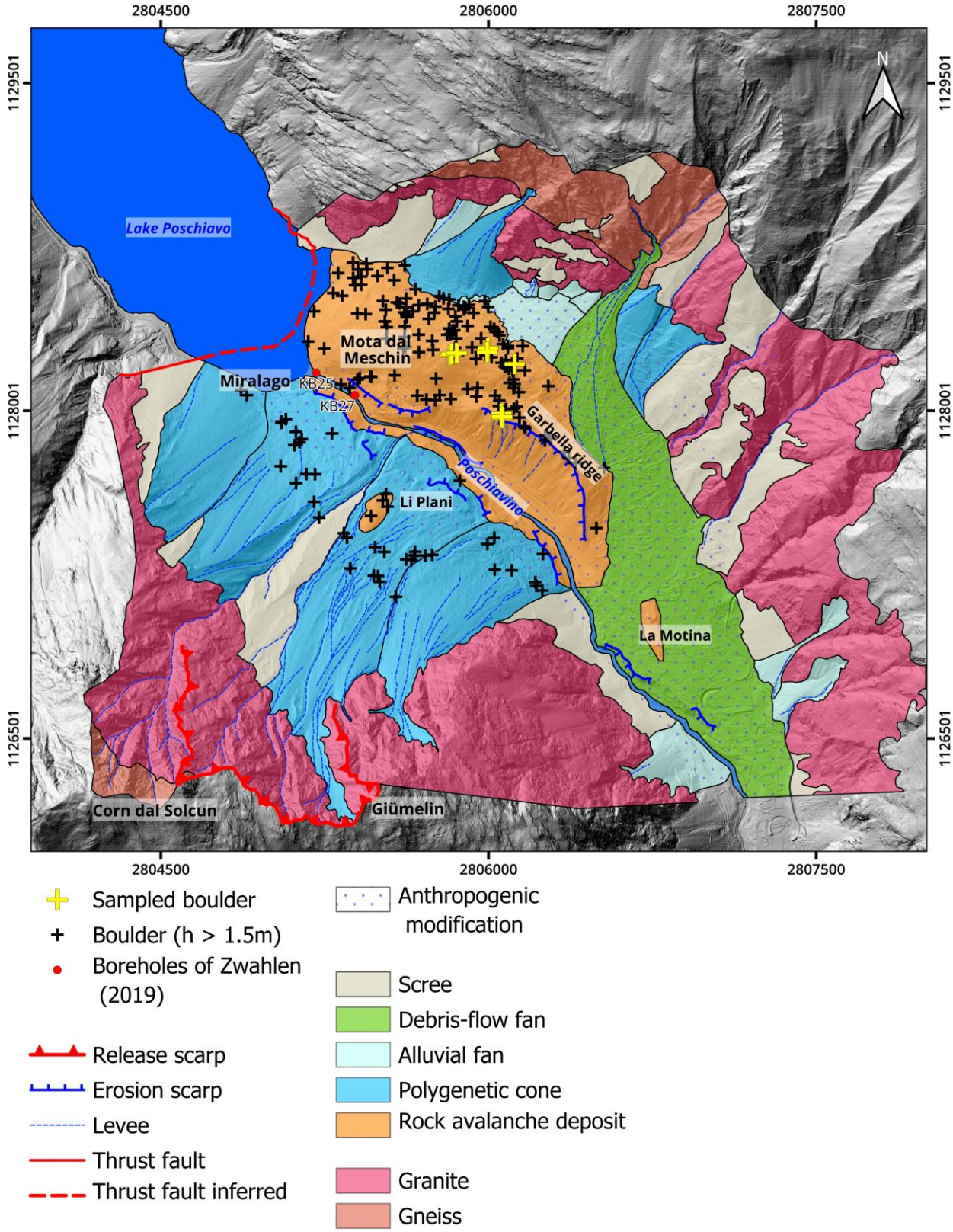

400

401 **Figure 4**. Surficial geology map of the study area.

402

Two additional, smaller bodies mapped as rock avalanche deposits occur away from the main Mota dal Meschin landform. One is located near La Motina, approximately 0.2 km southeast from the main deposit, and the other occurs near Li Plani, approximately 0.3 km southwest from the Mota dal Meschin landform (Figure 4). Taken together, the three mapped bodies extend approximately 2.5 km in a northwest–southeast direction and up to 1.15 km in a northeast–southwest direction. Their elevations range from approximately 860 m a.s.l. at the lowest distal occurrence to 1157 m a.s.l. on Mota dal Meschin. The main deposit is bordered by Poschiavo Lake to the northwest, polygenetic cones to the southwest, the Poschiavino River to the south and southeast, and debris-flow deposits to the east. Parts of the main deposit and adjacent valley-floor landforms show substantial anthropogenic modification. The study area covers around 9.1 km^2, and within this area around 1.75 km^2 show anthropogenic modification.

A total of 211 boulders higher than 1.5 m were mapped throughout the study area. Their spatial distribution is strongly heterogeneous. Most larger boulders, with a total of 152 boulders, occur on the broad upper surface of Mota dal Meschin and along the Garbella ridge, whereas fewer large boulders occur on the isolated deposits and adjacent polygenetic cone surfaces (Figures 4 and 5). The smaller deposit close to Li Plani has 4 boulders higher than 1.5 m and the deposit close to La Motina has no boulders of that size. Although the deposit near Li Plani has less boulders, the spatial density is higher with 237 boulders/km^2 than for the main deposit with 148 boulders/km^2. The boulders present outside of the rock avalanche deposit are mainly located on the polygenetic cones southwest of the Mota dal Meschin. Whether these two deposits represent isolated surface remnants, material incorporated into younger deposits, or unrelated slope-derived blocks is evaluated in the discussion below.

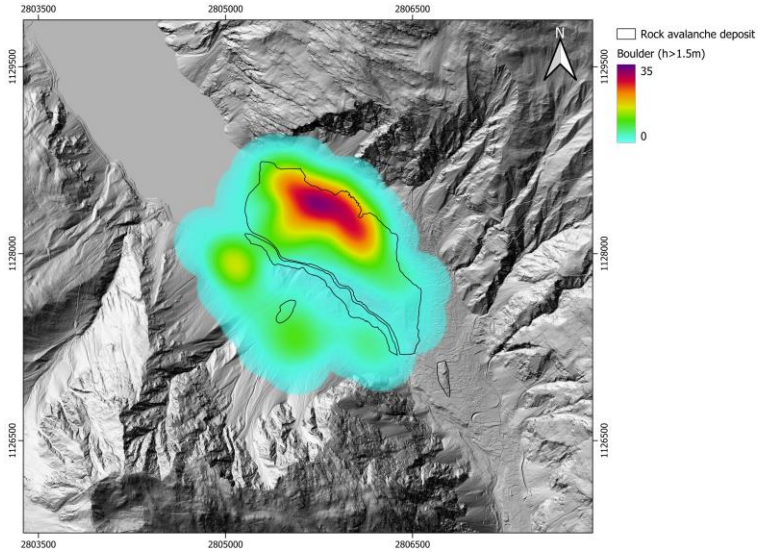

Figure 5. Distribution of the boulders larger than 1.5 m across the study area. The heatmap is generated in QGIS® with kernel density estimation (KDE) and using a search radius of 300 m.

The boulders are predominantly angular and range from approximately 0.5 m to more than 5 m in height (Figure 6). The largest blocks occur mainly on the flatter parts of Mota dal Meschin, while the boulders associated with the Li Plani deposit are generally smaller and do not exceed approximately 2 m in height. At the outcrops in the gravel pit (Mota di Miralago SA), large angular blocks locally form a clast-supported openwork fabric with conspicuous voids between adjacent clasts. Clasts strongly vary in size from a few cm to m in scale and were very angular and visibly broken up. In between the large clasts, smaller, mm sized broken pieces and finer rock-dust is creating a matrix. The outcrops show no visible stratification or sorting. No laterally continuous till unit was observed overlying the mapped rock avalanche deposit and no striated clasts were found.

The release scarp is located on the southwestern valley flank between Giümelin and Corn dal Solcun, at elevations of approximately 1800–2350 m a.s.l. (Figure 4). It is developed within crystalline bedrock comprising granite and gneiss and lies in a structurally complex area crossed by mapped thrust faults (Staub 1946; ©Federal Office of Topography Swisstopo 2014). The release area is approximately 1.1 km long and around 1.5 km wide. It covers an area of around 1.3 km^2 and faces toward northeast.

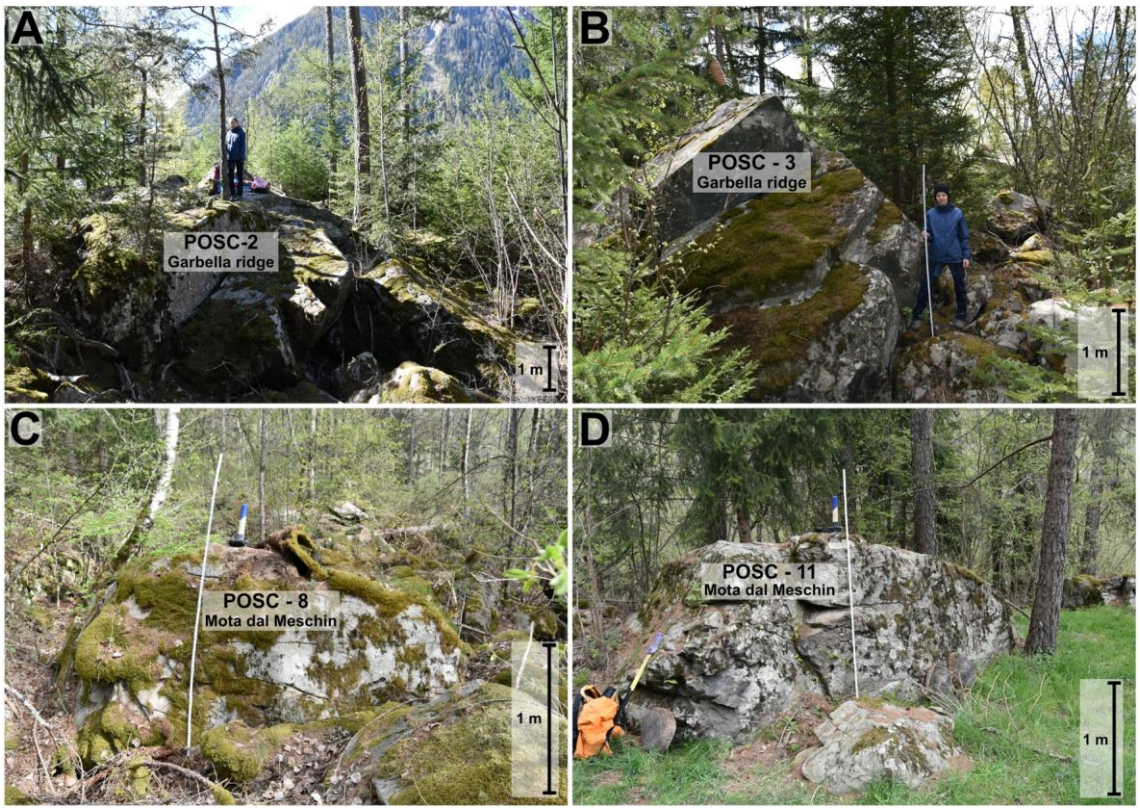

Figure 6. Photographs from four sampled boulders for surface exposure dating using ^{10}Be: **A** POSC-2, Garbella ridge, view southeast; **B** POSC-3, Garbella ridge, view south; **C** POSC-8, Mota dal Meschin, view northeast; **D** POSC-11, Mota dal Meschin, view north.

Boulder lithology and thin-section analysis

The mapped boulders comprise granitoid and gneissic lithologies that differ primarily in the intensity of their metamorphic fabric. Most boulders are massive to moderately foliated, with foliation spacing ranging from approximately 20 to 70 cm. A smaller group is strongly foliated or schistose, with foliation spacing of less than 5 cm, while some boulders show no macroscopically visible foliation. Thin-section analysis shows that both field-defined boulder groups are composed predominantly of quartz, feldspar and mica (Figure 7). No systematic difference in mineral assemblage was observed between the two groups; their distinction is mainly textural and reflects differences in foliation intensity and mineral alignment. The reference sample from the northeastern valley flank is strongly foliated, whereas the sample from the southwestern flank displays a weaker foliation. Both reference samples nevertheless have broadly similar mineral assemblages to the sampled boulders. Thus, the petrographic groups are differentiated principally by rock fabric rather than by mineral composition.

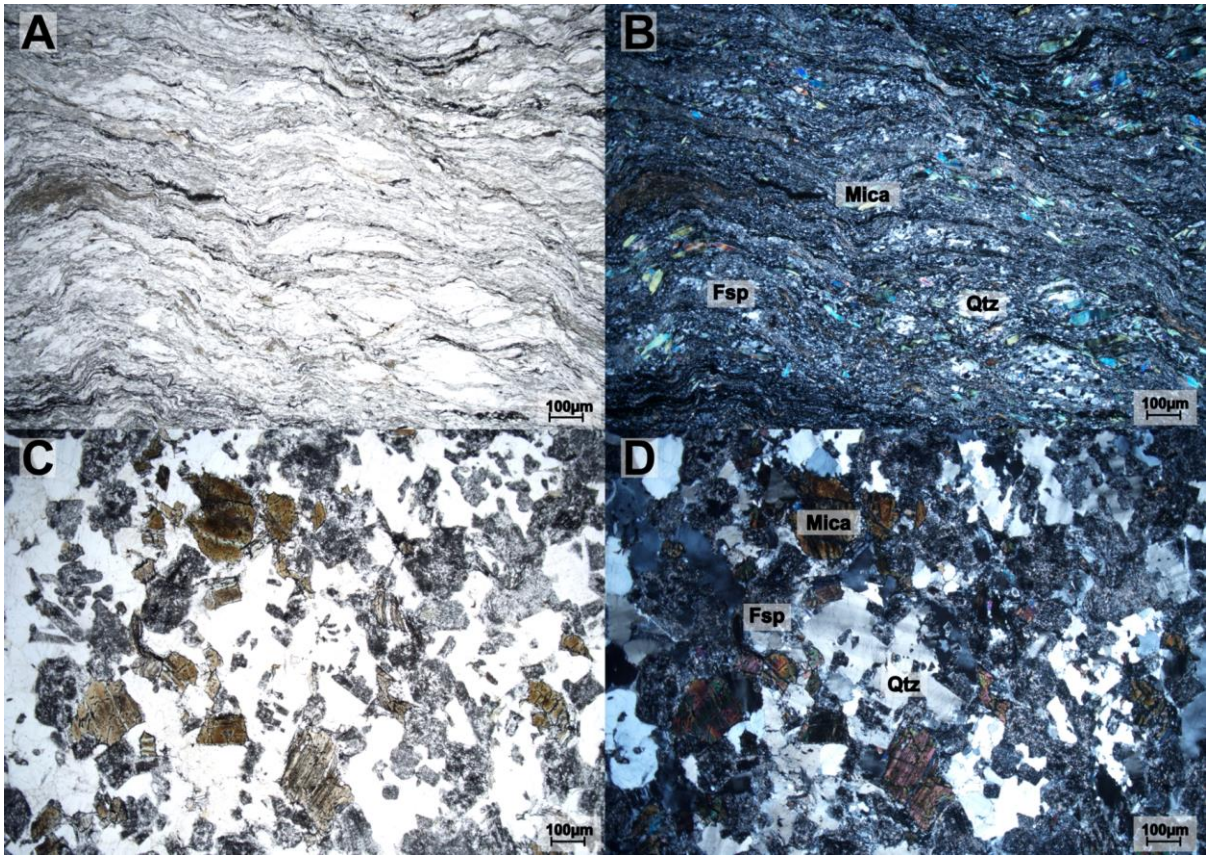

Figure 7. Microphotographs from the two different boulder categories. **A** visible schistosity under plane-polarised light; **B** visible schistosity under cross-polarised light; **C** no visible foliation under plane-polarised light; **D** no visible foliation under cross-polarised light.

Chronology

The amount of dissolved quartz, ^{9}Be carrier mass, measured ^{10}Be/^{9}Be ratios and associated analytical uncertainties, ^{10}Be concentrations and calculated exposure ages within 1σ uncertainties are reported in Table 2. ^{10}Be concentrations from the boulder surfaces in the Poschiavo rock avalanche deposit range from (10.48 ± 0.30) x 10^4 at/g to (11.79 ± 0.39) x 10^4 at/g, corresponding to erosion-corrected exposure ages of 10.8 ± 0.3 ka to 11.5 ± 0.4 ka (Figure 8). Ages are reported with 1σ uncertainties which include analytical uncertainties but exclude production rate uncertainty. External uncertainties, including production rate uncertainty, are given in parentheses in Table 2 following Balco et al. (2008).

The erosion-corrected exposure ages were additionally analysed using the Probabilistic Cosmogenic Age Analysis Tool, P-CAAT (Dortch et al. 2022). The analysis used the external 1σ uncertainty of each sample and the median absolute deviation–derived bandwidth estimator, yielding an optimized bandwidth of 0.329 ka. The resulting probability-density distribution is unimodal, with no statistically identified outliers, and yields a combined event age of 11.1 ± 0.5 ka for the nine boulders (Figure 9). The complete P-CAAT statistics are provided in the inset of Figure 9.

Table 2. Cosmogenic ^{10}Be data of the boulder samples from the Poschiavo Valley. Numbers in parenthesis for the erosion corrected exposure age are the external uncertainties.

Sample name	Quartz dissolved (g)	^{9}Be spike (mg)	AMS ratio (×10^{-13})	Error in AMS ratio (%)	^{10}Be (10^4 at/g)	Erosion corrected exposure age (ka) (ε = 1.0 mm ka^{-1})
POSC-1	35.39090	0.229	2.43 ± 0.07	2.9%	10.48 ± 0.30	10.8 ± 0.3 (0.9)
POSC-2	35.04050	0.247	2.27 ± 0.07	2.6%	10.69 ± 0.28	10.8 ± 0.3 (0.9)
POSC-3	35.06740	0.251	2.33 ± 0.07	2.9%	11.12 ± 0.32	11.4 ± 0.3 (0.9)
POSC-4	35.35110	0.247	2.32 ± 0.07	3.0%	10.84 ± 0.32	10.8 ± 0.3 (0.9)
POSC-5	35.01690	0.247	2.47 ± 0.07	2.7%	11.63 ± 0.31	11.5 ± 0.3 (0.9)
POSC-6	34.97580	0.248	2.49 ± 0.07	3.3%	11.79 ± 0.39	11.5 ± 0.4 (1.0)
POSC-7	35.00820	0.248	2.33 ± 0.07	2.7%	11.00 ± 0.29	11.1 ± 0.3 (0.9)
POSC-8	34.94840	0.249	2.35 ± 0.07	2.9%	11.22 ± 0.32	11.3 ± 0.3 (0.9)
POSC-11	35.92410	0.250	2.35 ± 0.07	3.0%	10.93 ± 0.33	11.0 ± 0.3 (0.9)

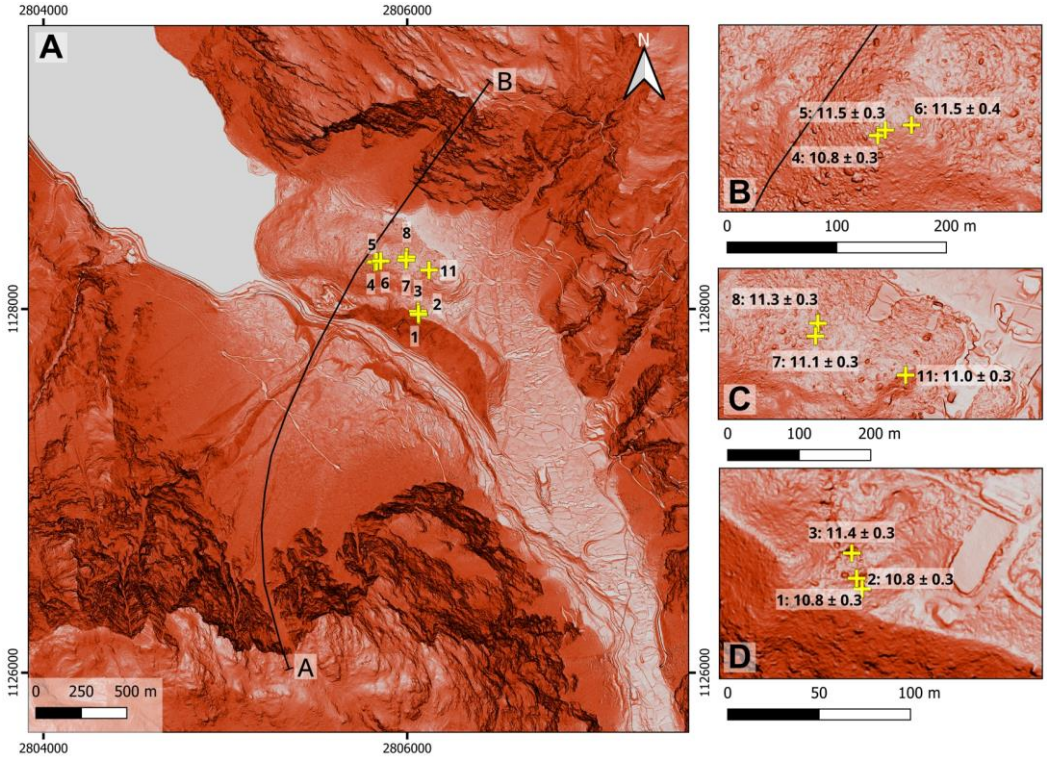

Figure 8. Red Relief from the study site. Yellow crosses mark the dated boulders using cosmogenic ^{10}Be. **A** Overview over the study site, the cross section from A to B is shown in Figure 10; **B-D** Zoomed-in areas displaying the ages in ka.

R^2	0.99737633
P-value	2.71E-128
BW Method	Mean
Bandwidth	0.32866667

Probability Height	0.891
Gauss. Age	11.1
Int. 1-Sigma	0.5
Ext. 1-Sigma	1.0
Ages (n)	9

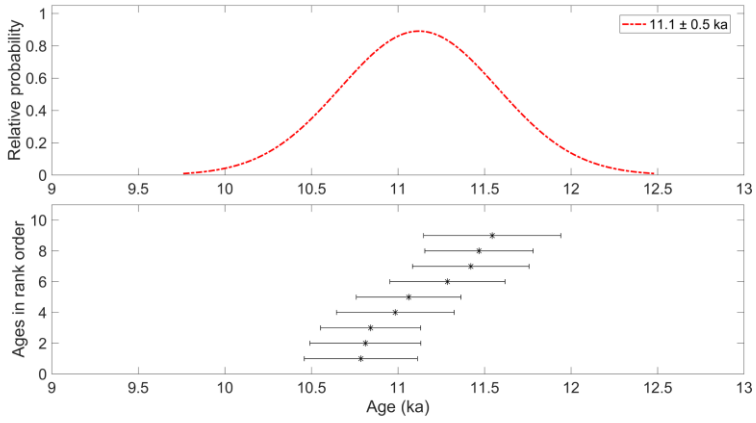

Figure 9. P-CAAT analysis of the 9 erosion-corrected ^{10}Be exposure ages. Upper inset tables report R^2, p-Value, Used Bandwidth method = Mean, bandwidth value (ka), probability height, Gaussian age and the 1σ internal and 1σ external uncertainties. Relative probability plot and ages plotted in rank order are shown below the tables. Sample information with internal and external uncertainties are displayed in table 2.

Emplacement dynamics

The preferred reconstruction of the pre-event landscape comprises a glacially overdeepened valley beneath the present southern part of Poschiavo Lake and a continuous slope across the release area between Giümelin and Corn dal Solcun (Figure 10). The reconstructed basal surface beneath the deposit was constrained by the borehole and geological-profile data of Zwahlen (2019), together with the present lake bathymetry and the morphology of the surrounding unaffected valley flanks. In borehole KB25, bedrock was encountered at approximately 943 m a.s.l., providing a direct constraint on the southeastern margin of the overdeepened basin. Borehole KB27 reached approximately 935 m a.s.l. without encountering bedrock and therefore provides only a maximum elevation, rather than a fixed bedrock depth, at that location.

Beneath the present lake, where no direct borehole control is available, the reconstructed basal surface reaches a minimum elevation of approximately 870 m a.s.l. The basin therefore deepens north-westward from the borehole-constrained area toward the present lake centre. The reconstructed valley cross-section has an asymmetric U-shaped geometry, with the rock avalanche deposit occupying the southeastern part of the overdeepened basin and extending across the former valley floor (Figure 10). Because the geometry below the lake is only indirectly constrained, this part of the reconstruction represents the largest source of uncertainty in the volume estimate.

In the release area, surficial deposits were removed and the pre-failure slope was reconstructed by interpolating between the preserved bedrock surfaces surrounding the mapped scarp. The reconstructed source extends between approximately 1800 and 2350 m a.s.l. and forms a continuous slope toward the valley floor. Only the source area, runout corridor, lake basin, and mapped depositional area were modified; terrain outside the inferred area affected by the rock avalanche was retained from the modern DEM.

The elevation difference between the reconstructed pre-depositional valley surface and the present-day surface yields a total mapped deposit volume of approximately 94 Mm^3. Assuming that fragmentation and bulking increased the volume of the deposited material by 20%, the corresponding intact source-rock volume is approximately 76 Mm^3. We assume an uncertainty of around 20% for the volume calculations due to the limitations of borehole data and unknown eroded rock avalanche mass since the deposition. This source volume was used to constrain the reconstructed pre-failure geometry and the initial mass distribution in the DAN3D® simulations.

A total of 32 DAN3D® simulations were performed using uniform- and spatially variable-material configurations (Table 3). The preferred simulations were selected according to their ability to reproduce the mapped distal and lateral limits of the rock avalanche deposits, the accumulation at Mota dal Meschin, and the occurrence of the smaller distal remnants at La Motina and Li Plani. Since we do not have any data on

549 deposits in the Lake, we tried to keep the modelled deposit at the overdeepening
550 minimal, in order to match the observed deposits as best as possible.

551 The two evaluated configurations used different ranges in the parameters. Based on
552 the parameter matrix summarized in Table 3, the uniform-material simulations
553 explored μ values of 0.15–0.21 and ξ values of 500–800. In the spatially variable
554 simulations, μ ranged from 0.20 to 0.23 for bedrock and from 0.16 to 0.20 for valley-
555 floor sediments and used the same ξ values of 500–800.

556 **Table 3.** Overview over the input parameters of some simulations made in DAN3D®.
557 Parameters for the best fit simulations are shown in grey.

Simulation	Material type	Behaviour	Unit weight (kN/m^3)	Friction coefficient μ	Turbulence coefficient ξ (m/s^2)	Internal friction angle (°)
V1	Uniform	Voellmy	20	0.15	500	35
V2	Uniform	Voellmy	20	0.21	500	30
V3	Uniform	Voellmy	20	0.20	800	30
V4	Uniform	Voellmy	20	0.18	800	30
V5 (Figure V11)	Uniform	Voellmy	20	0.19	800	30
V6	Uniform	Voellmy	20	0.16	500	30
V7	Uniform	Voellmy	20	0.17	500	30
V8	Uniform	Voellmy	20	0.18	500	30
V9	Uniform	Voellmy	20	0.19	500	30
V10	Uniform	Voellmy	20	0.18	600	30
V11 (Figure 11)	Uniform	Voellmy	20	0.19	600	30
V12	Uniform	Voellmy	20	0.17	700	30
V13 (Figures 11 and 12)	Uniform	Voellmy	20	0.18	700	30
V14	Uniform	Voellmy	20	0.17	600	30
V15 Multimat	Bedrock	Voellmy	20	0.21	800	30
	Sediments	Voellmy	20	0.18	800	30
V16 Multimat	Bedrock	Voellmy	20	0.20	800	30
	Sediments	Voellmy	20	0.19	800	30
V17 Multimat	Bedrock	Voellmy	20	0.20	800	30
	Sediments	Voellmy	20	0.18	800	30
V18 Multimat	Bedrock	Voellmy	20	0.22	800	30
	Sediments	Voellmy	20	0.18	800	30
V19 Multimat	Bedrock	Voellmy	20	0.21	800	30
	Sediments	Voellmy	20	0.20	800	30
V20 Multimat (Figure 11)	Bedrock	Voellmy	20	0.21	800	30
	Sediments	Voellmy	20	0.19	800	30
V21 Multimat	Bedrock	Voellmy	20	0.21	800	30
	Sediments	Voellmy	20	0.17	800	30
V22 Multimat	Bedrock	Voellmy	20	0.22	800	30
	Sediments	Voellmy	20	0.17	800	30
	Bedrock	Voellmy	20	0.21	800	30

V23 Multimat	Sediments	Voellmy	20	0.18	500	30
V24 Multimat	Bedrock	Voellmy	20	0.20	500	30
	Sediments	Voellmy	20	0.17	500	30
V25 Multimat	Bedrock	Voellmy	20	0.21	500	30
	Sediments	Voellmy	20	0.18	500	30
V26 Multimat	Bedrock	Voellmy	20	0.21	500	30
	Sediments	Voellmy	20	0.17	500	30
V27 Multimat	Bedrock	Voellmy	20	0.21	500	30
	Sediments	Voellmy	20	0.16	500	30
V28 Multimat	Bedrock	Voellmy	20	0.22	500	30
	Sediments	Voellmy	20	0.17	500	30
V29 Multimat	Bedrock	Voellmy	20	0.23	500	30
	Sediments	Voellmy	20	0.17	500	30
V30 Multimat	Bedrock	Voellmy	20	0.23	500	30
	Sediments	Voellmy	20	0.18	500	30
V31 Multimat	Bedrock	Voellmy	20	0.23	500	30
	Sediments	Voellmy	20	0.19	500	30
V32 Multimat (Figure 11)	Bedrock	Voellmy	20	0.23	500	30
	Sediments	Voellmy	20	0.16	500	30

In the best fitting uniform-material simulation (Table 3; V13), the entire runout path was represented using a single Voellmy rheology with a basal friction coefficient of μ=0.18 and a turbulence coefficient of ξ=700 ms^{-2}. The internal friction angle and unit weight of the moving mass were fixed at 30° and 20 kNm^{-3}, respectively. The modelled mass reached a maximum velocity of 123 $ms^{-1}$and travelled a maximum distance of approximately 1650 m. The final modelled deposit has a mean thickness of 32 m and a maximum thickness of 62 m. Motion had effectively ceased after approximately 450 s.

In the best fitting spatially variable configuration (Table 3; V20), separate basal-friction coefficients were assigned to the bedrock-dominated slope and the sediment-covered valley floor. The preferred simulation used μ=0.21 for the bedrock path and μ=0.19 for the valley-floor sediments, with a turbulence coefficient of ξ=800 ms^{-2} assigned to both domains. The internal friction angle and unit weight were again fixed at 30° and 20 kNm^{-3}. This simulation produced a higher maximum velocity of 139 ms^{-1}, but a slightly shorter maximum runout distance of 1610 m. The final deposit has a mean thickness of 33 m and a maximum thickness of 62 m, and motion had effectively ceased after approximately 360 s.

Despite differences in the assigned basal parameters, the two preferred simulations produce similar final depositional geometries. Their mean deposit thicknesses differ by <1 m and their maximum thicknesses by <1 m. The uniform-material simulation produces a slightly longer runout, whereas the spatially variable simulation reaches a higher peak velocity and requires approximately 90 s less to reach its final state. The uniform-material simulation (V13) is slightly more fitting to today's situation visible in

the field, since the deposit ends closer to La Motina compared to the spatially variable simulation (V20). The deposit closer to Li Plani is also slightly more thick in the uniform-material simulation than in the spatially variable one, which suits the observed deposit better (Figure 11). Both simulations reproduce the main deposit, the Mota dal Meschin. They also manage to reproduce a small deposit close to Li Plani, like observed in the field and the simulated deposit reaches La Motina, which is the location of the third found deposit in the field. A large accumulation did form in the overdeepened basin below today's lake surface, which we cannot further evaluate with the known data. Additionally, both simulations show that all three deposits are connected to each other. This is not visible in the field today anymore. All simulations failed to reproduce the Garbella ridge.

The initial evolution of the best fitting simulation (V13) shows that of the mass accelerates downslope through the source area and reaches the valley floor within 50s. The material then spreads laterally and begins to decelerate as it enters the overdeepened valley basin. Between 50 s and 100 s, the simulation shows substantial accumulation within the reconstructed basin, including deposition beneath the area presently occupied by Lake Poschiavo. After the first 100 s, the process slows down and the mass slowly begins to settle. This subsequent movement mainly involves redistribution and gradual thickening of the deposit rather than continued extension of the runout. Only small parts of the mass slowly flow further in downvalley direction to La Motina until at 450s a stable position on the valley floor is reached (Figure 12). The corridor towards the overdeepening was able to hold back a lot of the material, which had the tendency to travel further downvalley towards La Motina.

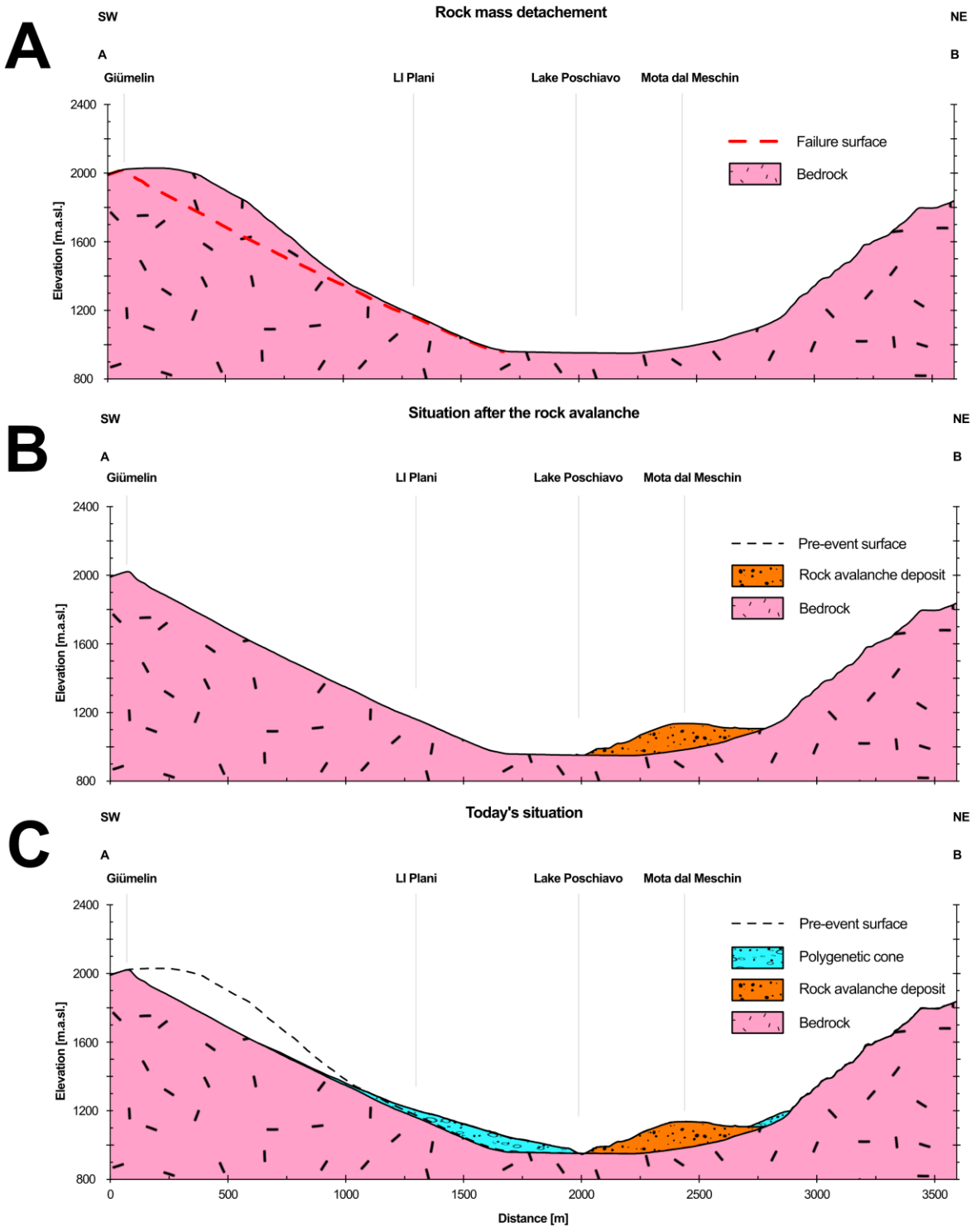

Figure 10. Cross sections from Southwest to Northeast in the Poschiavo valley, illustrating the rock avalanche in 3 timesteps. **A** Situation before the failure with the indicated failure surface (simplified bedrock); **B** Situation immediately after the failure; **C** Situation today in the Poschiavo Valley with the indicated pre-event surface.

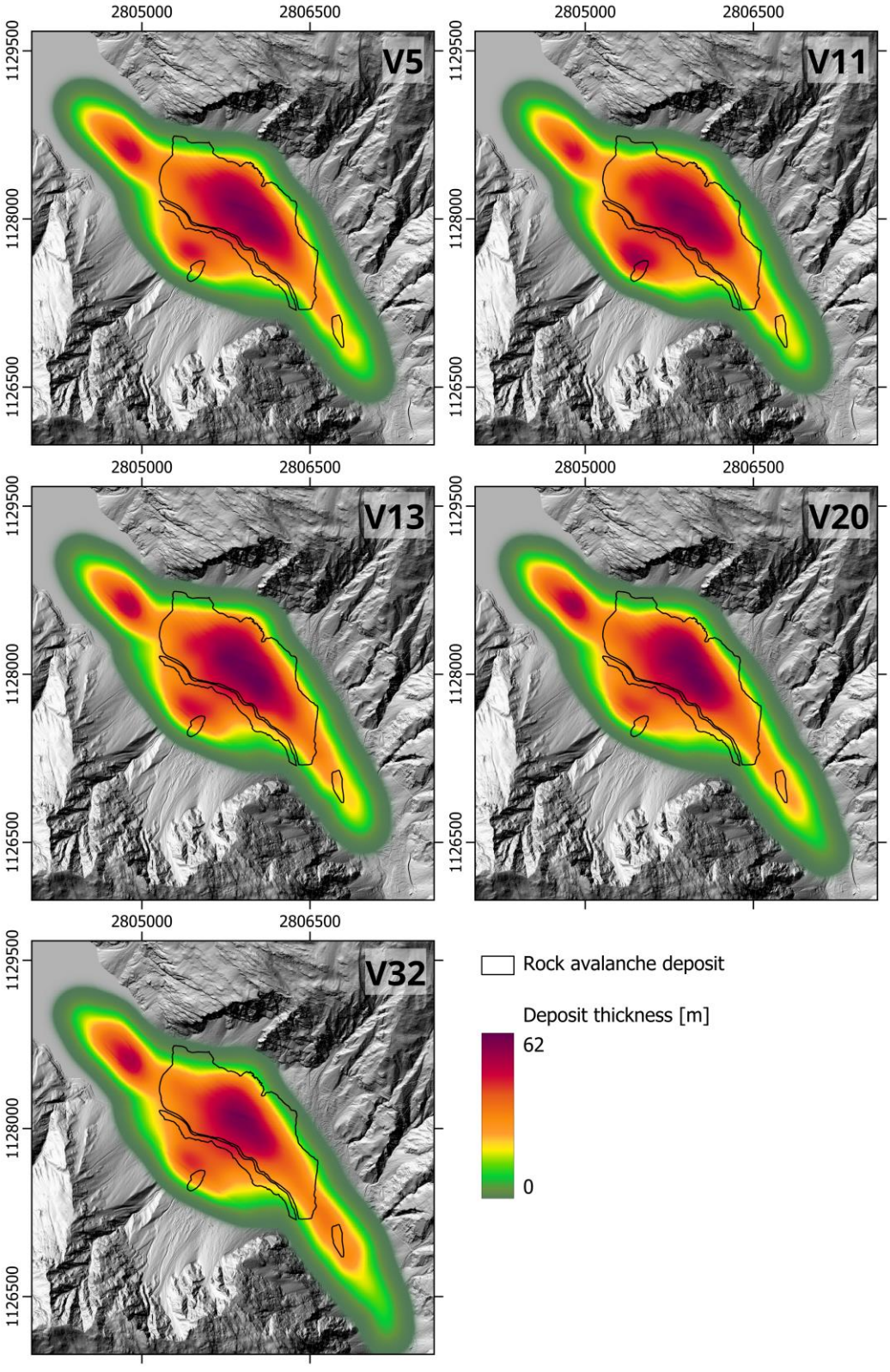

Figure 11. Thickness and extent after final deposition for five simulations made with DAN3D® using a uniform-material approach (V5, V11 and V13) and spatially variable approach (V20, V32). The best fitting simulations are represented in the middle (V13, V20), whereas the others (V5, V11, V32) show worse fits.

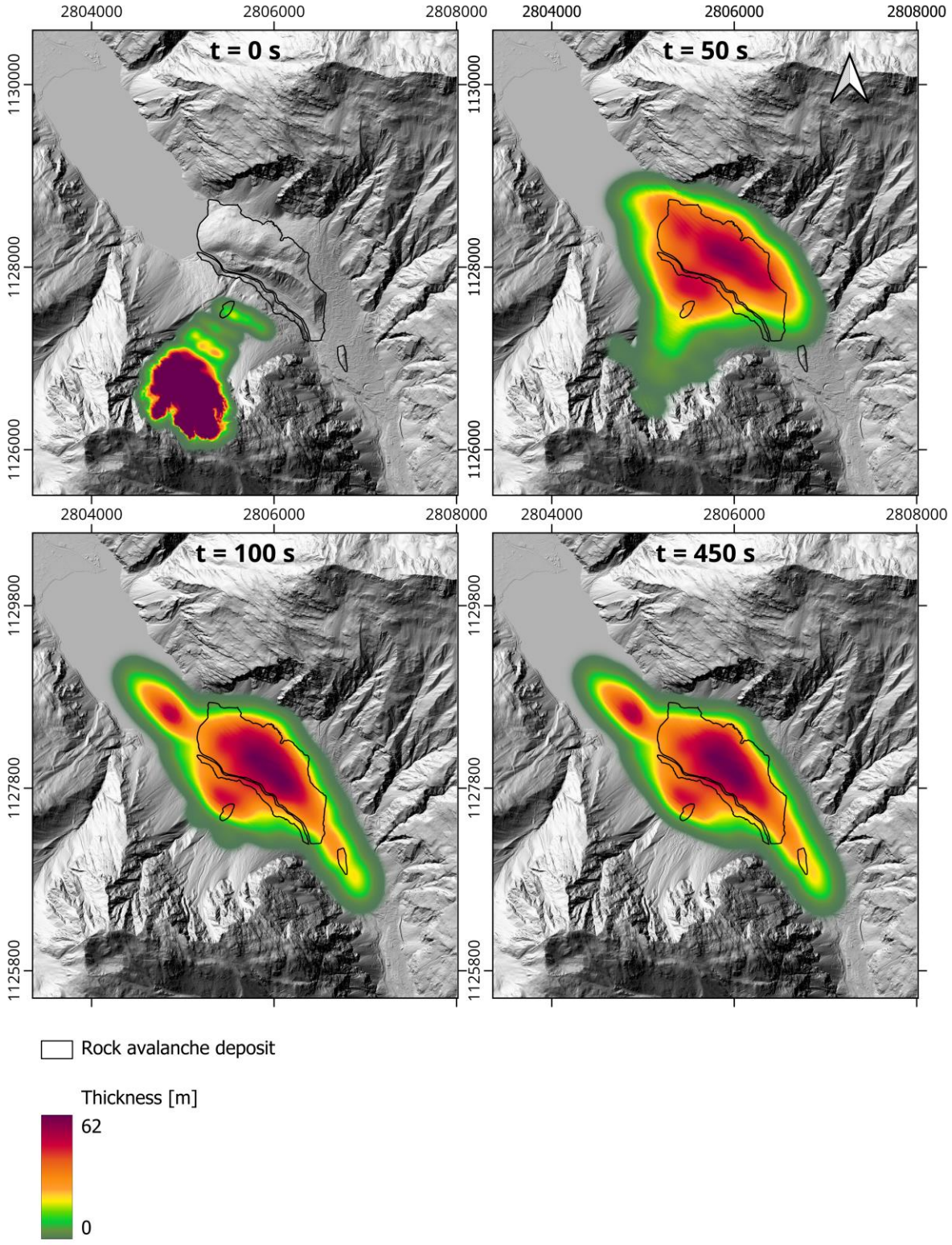

616

617 **Figure 12.** Thickness and extent during different timesteps from the best fitting
618 simulation made in DAN3D® (V13).

Discussion

Origin and event history of the Mota dal Meschin deposit

The combined geomorphological, sedimentological, and geochronological evidence supports a rock avalanche origin for the Mota dal Meschin deposit. Its irregular surface morphology, abundance of large angular boulders, and locally preserved clast-supported openwork fabric contrast with the commonly compact, matrix-supported diamicton characteristic of till (cf. Porter and Orombelli 1980; Akçar et al. 2012). In addition, no laterally continuous till unit was identified overlying the exposed parts of the deposit, and the investigated clasts show no clear evidence of glacial abrasion or transport. Although the absence of striations is not diagnostic in itself, particularly in resistant granitoid and gneissic lithologies, the combined landform and sedimentological evidence is more consistent with rapid rock avalanche emplacement than with primary deposition by a glacier. Similar interpretive difficulties have been documented in Alpine and other formerly glaciated mountain valleys, where rock avalanche deposits may be mistaken for glacial deposits or subsequently modified by glacial, fluvial, and periglacial processes (Porter and Orombelli 1980; Akçar et al. 2012; Cook et al. 2013; Schleier et al. 2015; Pfiffner et al. 2023; Bucher et al. 2024; Rubin et al. 2026).

Our mapping therefore revises earlier interpretations that assigned parts of the mapped area to glacial deposits. Staub (1946) and Zwahlen (2019) mapped till overlying parts of the rock avalanche deposit, whereas the ©Federal office of topography Swisstopo (2023) classified the entire blocky deposit as till. The surficial deposits adjoining Mota dal Meschin are interpreted here as a combination of rock avalanche material, deposits of debris-flow and polygenetic cones, and alluvial sediments rather than as an extensive and continuous till cover. This reinterpretation is based primarily on surface morphology, sedimentary characteristics, and field relationships, because continuous exposures of the contacts between these units are rare. Consequently, the subsurface distribution of the rock avalanche deposit remains uncertain where it is concealed by younger debris-flow and alluvial sediments. Comparable revisions have been necessary elsewhere in the Alps. In the Obernberg Valley, transverse ridges formerly interpreted as Lateglacial moraines were reclassified as rock avalanche deposits on the basis of their internal structure, geomorphology, and chronology (Ostermann et al. 2012). Likewise, the Lurnigalp deposit was originally mapped as till before being reinterpreted using integrated mapping, sedimentary petrology, exposure dating, and runout modelling (Bucher et al. 2024).

The preservation of large angular blocks and a locally openwork fabric, together with the absence of a laterally continuous till unit overlying the exposed deposit, provides no evidence that the Mota dal Meschin deposit was substantially overridden or reworked by glacier ice after emplacement. Documented Alpine examples show that interaction with glacier ice may redistribute rock avalanche debris, modify its surface

morphology, and incorporate the material into moraine complexes, as observed in the upper Val Ferret of the Mont Blanc Massif (Deline and Kirkbride 2009; Akçar et al. 2012). Conversely, at the Tamins rock avalanche, the preservation of metre-scale blocks and closed depressions unfilled by till was used as evidence against the passage of a younger glacier over the deposit (Pfiffner et al. 2023). The corresponding preservation of coarse surface morphology at Mota dal Meschin similarly argues against extensive post-emplacement glacier overriding. However, the absence of such evidence does not exclude localized contact with glacier ice or the persistence of small glaciers in higher tributary catchments. A comparable configuration was reconstructed at Lurnigalp, where a small glacier may have occupied the upper cirque while the valley floor remained ice-free during rock avalanche emplacement (Bucher et al. 2024). The available observations therefore suggest that the main Poschiavo Valley near Miralago was probably ice-free when the deposit was emplaced and show no evidence of subsequent extensive glacier overriding, consistent with the regional reconstruction of Burga (1987).

The nine cosmogenic ^{10}Be exposure ages define a statistically coherent, unimodal population with a combined age of 11.1 ± 0.5 ka. The agreement between exposure ages from the main Mota dal Meschin deposit and the Garbella ridge indicates that these landforms were exposed contemporaneously (Figure 8). The limited age scatter and absence of a pronounced older tail indicate that large and heterogeneous contributions from inherited ^{10}Be were not dominant. However, a small and broadly similar inherited component in all sampled boulders could shift the entire age population toward older values without producing statistically identifiable outliers. Pre-failure inheritance is particularly relevant to rock avalanche boulders because large blocks may originate from shallow parts of the source slope that were exposed to cosmic radiation before failure (Akçar et al. 2012, 2014; Hilger et al. 2019). Experimental studies demonstrate that inheritance may be negligible in some recently deposited boulders (Abbühl et al. 2009), but measurable inherited ^{10}Be has also been documented in historical rock avalanche deposits (Akçar et al. 2014; Hilger et al., 2019). Conversely, exhumation, shielding, erosion, toppling, or other post-depositional processes may produce anomalously young apparent exposure ages (Akçar et al. 2011; Balco 2011; Heyman et al. 2011, 2016). The coherent Poschiavo dataset therefore provides a robust estimate of the principal Surface exposure age, although minor systematic inheritance or post-depositional modification cannot be excluded completely.

The coherent surface exposure chronology supports that the Mota dal Meschin deposit and Garbella ridge were emplaced, or stabilized at the surface, during one principal catastrophic failure. Statistical agreement among the exposure ages is consistent with a common event but does not independently prove that no additional failures occurred. This interpretation differs from Zwahlen's (2019) reconstruction of several rock avalanche units within the Miralago borehole succession, although the two datasets are not necessarily incompatible. Our chronology constrains the time since the sampled boulder surfaces became exposed and remained sufficiently stable, whereas

the boreholes record buried stratigraphic units that cannot presently be correlated directly with each mapped surface deposit (Gosse and Phillips 2001; Ivy-Ochs and Kober 2008; Schaefer et al. 2022). The borehole succession may therefore preserve smaller secondary failures, reworked rock avalanche material, or additional mass-movement events that are no longer exposed at the surface. Resolving these alternatives requires independent dating of the individual buried units and a more direct stratigraphic correlation between the boreholes and the mapped surface deposits.

Taken together, our results support a principal rock avalanche event at 11.1 ± 0.5 ka that formed the preserved Mota dal Meschin deposit and Garbella ridge. The geomorphological and sedimentological evidence indicates that emplacement probably occurred under ice-free conditions in the main Poschiavo Valley and provides no indication of substantial post-emplacement glacier overriding. However, the available Surface exposure chronology does not independently exclude smaller secondary failures or reworked mass-movement units represented only in the subsurface succession.

Source and emplacement dynamics

The lithological composition of the Mota dal Meschin boulders is compatible with a source within the crystalline rocks of the Bernina Nappe. Both the sampled boulders and the reference bedrock contain quartz, feldspar, and mica, with variations mainly expressed in foliation intensity. However, similar lithologies crop out on both sides of the Poschiavo Valley, and the petrographic observations alone cannot identify the release area unambiguously. A source on the southwestern valley flank is nevertheless favoured by the combined geomorphological, topographic, and modelling evidence. The release area between Giümelin and Corn dal Solcun provides sufficient relief and volume to accommodate the reconstructed failed mass, whereas the northeastern flank is too restricted to contain a source of comparable size (Figures 4 and 10). Moreover, the geometry of the reconstructed release area and the simulated direction of movement are consistent with emplacement toward Mota dal Meschin. Comparable integrated approaches combining lithological provenance, source morphology, volume reconstruction, and runout modelling have been used to constrain source areas of other Alpine rock avalanches (Singeisen et al. 2020; Pfiffner 2022; Pfiffner et al. 2023; Bucher et al. 2024). Detailed mapping of source and deposit lithologies has, for example, been central to reconstructing the emplacement of the Flims and Tamins rock avalanches.

The reconstructed rock avalanche deposit has a present-day volume of approximately 94 Mm^3. Assuming that the deposited material expanded by 20% relative to the intact source rock (Abele 1974; Hungr and Evans 2004), this corresponds to an estimated source volume of approximately 76 Mm^3. This estimate is subject to considerable uncertainty because the original deposit has been modified by river incision, fan deposition, and human activity, while the pre-failure valley-floor topography is only partly constrained by borehole data. In particular, the depth and geometry of the

overdeepened basin beneath present-day Lake Poschiavo remain uncertain. Reconstructions of other large Alpine failures similarly show that inferred volumes depend strongly on the representation of the pre-failure source slope, the buried valley floor, and the extent of eroded or concealed deposits (Singeisen et al. 2020; Pfiffner, 2022; Pfiffner et al. 2023; Bucher et al. 2024; Dieleman et al. 2025). The reconstructed volume should therefore be regarded as a first order estimate rather than a precise measure of the failed mass. Palaeotopographic reconstruction is explicitly identified as critical to source-volume estimation in the Flims rock avalanche (Pfiffner 2022).

Both preferred DAN3D® simulations reproduce the first-order extent and geometry of the mapped deposits and support rapid emplacement from the southwestern source area. In the simulations, the failed mass reached the valley floor after approximately 50 s, spread laterally across the overdeepened basin, and accumulated beneath the area now occupied by the southern part of Lake Poschiavo. Movement subsequently continued toward the mapped distal deposits before gradually ceasing after approximately 6–8 min. DAN3D® is a depth-averaged numerical model developed to simulate the motion and deposition of rapid landslides over three-dimensional terrain (Hungr and McDougall 2009). The modelled sequence demonstrates that the preserved deposit geometry can be produced by a single large failure and therefore supports the one-event interpretation derived from the surface exposure chronology. However, successful numerical reproduction by a single release scenario shows that such an event is mechanically plausible; it does not independently exclude smaller failures before or after the principal event.

The uniform-material and spatially variable-material simulations produce broadly similar final deposit geometries, despite differences in the assigned basal parameters. The spatially variable simulation reaches a slightly higher maximum velocity, whereas the uniform-material simulation extends marginally less toward the southeast. Nevertheless, both models generate comparable mean and maximum deposit thicknesses and reproduce the main accumulation zone within the valley-floor basin. The limited difference between the simulations indicates that the broad runout pattern is controlled primarily by the reconstructed source geometry and valley topography rather than by the distinction between the two basal-material domains. However, calibration-based runout models commonly permit several parameter combinations to reproduce broadly similar deposit extents, and fitted parameters are therefore rarely unique (Aaron et al. 2022). Similar behaviour has been observed in back-analyses of Alpine rock avalanches using DAN3D® and related approaches (Singeisen et al. 2020; Pfiffner et al. 2023; Bucher et al. 2024; Dieleman et al. 2025; Rubin et al. 2026).

The preferred simulations do not require exceptionally low effective basal-friction values for the valley-floor sediments. This contrasts with Alpine rock avalanches in which water-saturated or mechanically weak substrates have been inferred to enhance mobility. At Flims, for example, mobilization and possible liquefaction of water-saturated glaciolacustrine and fluvial sediments contributed to long runout, entrainment, and substantial modification of the valley floor (Pfiffner 2022). Strong

787 substrate weakening was also required in the preferred reconstruction of the Sierre
788 landslide (Rubin et al. 2026). However, the calibrated DAN3D® parameters represent
789 bulk effective behaviour and cannot be used to reconstruct the original water content
790 or mechanical state of the Poschiavo valley-floor sediments directly. The modelling
791 therefore shows that pronounced substrate weakening is not required to reproduce
792 the observed runout, but it does not demonstrate that the valley floor was dry or
793 completely unsaturated at the time of failure.

794 The mapped bodies at Mota dal Meschin, La Motina, and Li Plani are interpreted as
795 remnants of a more extensive and originally more continuous rock avalanche deposit
796 (Figures 4 and 12). This interpretation is supported by their comparable morphology
797 and lithology and by the simulated distribution of material across the valley floor.
798 Following emplacement, incision by the Poschiavino River likely removed part of the
799 deposit and separated the surviving remnants. Additional portions were subsequently
800 buried or reworked by the debris-flow fan east of Mota dal Meschin and by polygenetic
801 cones near Li Plani. Comparable modification of Alpine rock avalanche deposits by
802 river incision, fan aggradation, substrate entrainment, and younger mass movements
803 has been documented at Kandersteg, Tamins, Flims, and Lurnigalp (Singeisen et al.
804 2020; Pfiffner 2022; Pfiffner et al. 2023; Bucher et al. 2024; Dieleman et al. 2025). At
805 Flims, for example, river incision produced the Ruinaulta Gorge and exposed the
806 internal structure of the rock avalanche deposit (Pfiffner 2022). The present
807 discontinuous distribution therefore probably reflects substantial post-emplacement
808 modification rather than three entirely independent surface deposits. Nevertheless,
809 direct subsurface correlations between the isolated bodies are currently lacking, and
810 their original continuity remains an interpretation rather than a demonstrated
811 stratigraphic relationship.

812 By occupying the overdeepened valley floor, the rock avalanche probably obstructed
813 the Poschiavino River and influenced the subsequent development of Lake Poschiavo.
814 Formation of natural dams and upstream lakes is a common consequence of large
815 rock avalanches entering confined mountain valleys, although their longevity depends
816 on dam geometry, sediment composition, inflow, and subsequent overtopping or
817 incision (Costa and Schuster 1988). Alpine examples include the lakes impounded by
818 the Flims, Tamins, Oeschinensee, and Kandersteg rock avalanches (Köpfli et al.,
819 2018; Singeisen et al., 2020; Pfiffner, 2022; Pfiffner et al., 2023). The reconstructed
820 and modelled Poschiavo deposits indicate substantial accumulation within the present
821 lake basin and near Mota dal Meschin, where the rock avalanche mass may have
822 formed or reinforced a natural barrier. Two scarps on the opposite side of the valley
823 occur at elevations of approximately 1030 and 980 m a.s.l. and could record former
824 lake levels, but their interpretation as paleo-shorelines has not yet been confirmed.
825 The available evidence therefore suggests that the rock avalanche contributed to
826 valley obstruction and lake evolution, although the original dam geometry, the
827 magnitude and duration of lake-level changes, and the relationship between the event
828 and any pre-existing lake remain unresolved. Bathymetric, seismic-stratigraphic, or
829 additional borehole investigations would be required to test this interpretation. Flims

and Tamins provide particularly relevant Alpine examples of rock avalanche damming, lake formation, overtopping, and subsequent incision (Pfiffner et al. 2022; Pfiffner 2023).

Preconditioning, triggering, and Alpine context

The timing of the Poschiavo rock avalanche indicates that failure occurred after the main valley glacier had retreated from the Miralago sector. The retreat of an active glacier directly adjacent to the source slope is therefore unlikely to have been the direct trigger. Nevertheless, repeated Pleistocene glaciations probably exerted a strong long-term control on slope stability. Glacial incision and overdeepening steepen valley flanks and modify the gravitational stress field, while repeated cycles of glacial erosion, loading and unloading may progressively damage the rock mass and promote fracture growth (McColl 2012). Such delayed responses form part of the broader paraglacial adjustment of mountain landscapes, in which slope instability may persist for centuries to millennia after glacier retreat rather than occurring synchronously with deglaciation (Church and Ryder 1972; Ballantyne 2002; McColl and Davies 2013; McColl and Draebing 2019; Spreafico et al. 2021). Numerical studies in the Swiss Alps further indicate that repeated glacial cycles can generate progressive thermo-hydro-mechanical damage extending well beyond a simple loss of lateral ice support (Grämiger et al. 2017, 2018, 2020). The temporal separation between local deglaciation and failure at Poschiavo is therefore compatible with long-term glacial preconditioning but does not establish a direct causal link with the final phase of glacier retreat.

The geological structure of the southwestern valley flank may have provided an additional control on instability development. The reconstructed source area consists of foliated crystalline rocks of the Bernina Nappe, in which foliation planes, joints and pre-existing fracture zones may have favoured progressive deformation and the development of an internal or basal rupture surface. Structural control is common in large Alpine rock-slope failures, although its importance varies with discontinuity orientation, rock mass damage and slope geometry (Stead and Wolter 2015). At Köfels, for example, numerical reconstruction suggests a combination of block failure, shearing along persistent discontinuities and progressive development of internal shear zones, rather than failure along one simple pre-existing plane (Zangerl et al. 2021). Similar studies emphasize that glacially induced damage and subcritical fracture propagation may progressively reduce rock-mass strength before catastrophic failure (Brückl and Parotidis 2005; Grämiger et al. 2017; Spreafico et al. 2021). However, systematic measurements of foliation, joint orientation, fracture persistence and rock-mass strength are not yet available for the Poschiavo source area. Structural preconditioning is therefore plausible, but the initial failure mechanism cannot be reconstructed uniquely from the present topographic and petrographic evidence.

The timing of collapse at 11.1 ± 0.5 ka places the main Poschiavo event in the Early Holocene, shortly after the Younger Dryas-Holocene transition. The Younger Dryas in

872 the Alps was characterized by renewed glacier expansion and widespread periglacial
873 activity, but its internal climate was spatially and seasonally variable (Kerschner and
874 Ivy-Ochs 2008; Ivy-Ochs et al. 2009b, 2023b; Schindelwig et al. 2012; Koltai et al.
875 2021; Binaghi et al. 2025). The subsequent transition into the Holocene involved rapid
876 atmospheric warming, glacier downwasting and major reorganizations of snow,
877 permafrost and hydrological regimes (Le Roy et al. 2024; Nicolussi et al. 2026). These
878 changes could theoretically influence rock-slope stability through permafrost
879 degradation, weakening of ice-filled fractures, altered meltwater infiltration and
880 changes in groundwater pressure (Gruber and Haeberli 2007; McColl and Draebing
881 2019; de Palézieux and Loew 2019; Grämiger et al. 2020). Modern and
882 paleoenvironmental studies demonstrate that permafrost warming and glacier
883 recession can contribute to rock wall destabilization but also show that geological and
884 topographic predisposition remain essential controls (Gruber and Haeberli 2007;
885 Fischer et al. 2012; Gallach et al. 2018; McColl and Draebing 2019).

886 A climate-related contribution to failure is therefore conceivable, but it cannot be
887 demonstrated directly at Poschiavo with the current data. No independent evidence
888 currently constrains the former lower limit of permafrost, the presence of ice-filled
889 fractures, or an exceptional episode of precipitation or snowmelt at the source slope.
890 Moreover, climatic forcing usually acts by preparing or progressively weakening a
891 slope, whereas the final transition to catastrophic failure may result from a much
892 shorter hydrological, thermal or seismic perturbation. Studies of contemporary Alpine
893 rock failures similarly show that temperature and precipitation anomalies may precede
894 failure, but that their mechanical role is difficult to isolate from long-term fracture
895 development and rock-mass deterioration (Fischer et al. 2012; Paranunzio et al.
896 2016). The exposure age therefore establishes the climatic context of the Poschiavo
897 event but does not identify warming, permafrost degradation or increased groundwater
898 recharge as its immediate trigger.

899 A seismic trigger also remains possible. The Poschiavo Valley lies south of the
900 Engadine Valley and the Engadine Line, a major regional tectonic structure associated
901 with historical and palaeoseismic activity. The sedimentary sequence of Lake
902 Silvaplana, which is located around 30 km northwest of lake Poschiavo, records
903 several basin-wide mass-movement deposits and megaturbidites interpreted as
904 earthquake-related events during the Holocene (Bellwald et al. 2024). The oldest
905 inferred phase of seismic activity has a maximum age of 11,300 cal yr BP and broadly
906 overlaps with the uncertainty range of the Poschiavo exposure chronology. The
907 Engadine and Poschiavo Valley remain seismically active in the present day, however
908 most earthquakes have a magnitude <2 with only few reaching magnitudes up to 3.2
909 since 2002. (Swiss Seismological Service 2026). Regional examples show that
910 temporal coincidence between apparently synchronous rock avalanches and
911 independently reconstructed earthquakes can provide an argument for co-seismic
912 failure, as proposed for the two Rinderhorn events and the Oeschinensee rock
913 avalanche (Grämiger et al. 2016; Köpfli et al. 2018). However, the oldest Lake
914 Silvaplana event ages are only broadly constrained, and no coseismic deformation,

liquefaction feature or independently dated earthquake horizon has been identified at Poschiavo. The available evidence therefore demonstrates that strong regional seismicity was possible but does not permit correlation of the rock avalanche with an individual earthquake.

With a reconstructed deposit volume of approximately 94 Mm^3, the Poschiavo rock avalanche belongs to the larger post-LGM slope failures in the Alps, although it is substantially smaller than giant events such as Flims and Köfels. Its age adds to a growing record of large Alpine failures during the Lateglacial and Early Holocene. The Durchgangwald event occurred during the Younger Dryas, the Lurnigalp rock avalanche was dated to approximately 12.0 ± 2.0 ka, and the two Rinderhorn failures occurred at approximately 9.8 ± 0.5 ka (Bichler et al. 2016; Grämiger et al. 2016; Bucher et al. 2024). Other major Early Holocene events include Flims at approximately 9.4 ka, Köfels at approximately 9.5 ka and Tamins at 9.4 ka (Deplazes et al. 2007; Ostermann et al. 2012; Nicolussi et al. 2015; Pfiffner et al. 2023). These failures occurred in different lithologies, structural settings and glacial configurations, and their temporal relation to local deglaciation varies considerably. For example, the Rinderhorn and Köfels failures occurred several millennia after local ice retreat, indicating that direct glacier unloading is not required immediately before failure.

The chronological record also indicates that Alpine rock-slope instability was not restricted to the Lateglacial–Early Holocene transition. Periods of enhanced slope-failure activity have been identified during the Early Holocene (ca. 10.5–9.4 ka) and mid-Holocene (ca. 4.2–3.0 ka; Ivy-Ochs et al. 2017; Aksay et al. 2021). Repeated Holocene rock avalanches onto Brenva Glacier have been documented, and deposits previously attributed to a single Val Viola rock avalanche were recently interpreted as the products of three distinct mid-Holocene events (Deline et al. 2015; Longhi et al. 2024). Late Holocene failures such as Kandersteg and Oeschinensee further demonstrate that large Alpine rock avalanches occurred under markedly different climatic boundary conditions (Köpfli et al. 2018; Singeisen et al. 2020). Despite the apparent temporal clustering, the triggers of individual failures remain uncertain. Taken together, these records favour a model in which long-term slope preparation is controlled by site-specific combinations of topography, geological structure, glacial inheritance and progressive rock-mass damage, whereas the immediate trigger may differ among events.

The apparent concentration of large failures after deglaciation may also partly reflect preservation, recognition and dating biases. Rock avalanche deposits in formerly glaciated valleys can be buried by alluvial or lacustrine sediment, eroded by rivers, reworked by later glaciers or incorrectly mapped as glacial deposits. Such processes preferentially remove or conceal older events and may produce an apparently young landslide inventory (Prager et al. 2008; Pánek 2019; McColl 2020). The reinterpretation of Lurnigalp from till to rock avalanche material and the recognition of several separate failures at Val Viola illustrate how improved mapping and dating can alter regional event inventories (Bucher et al. 2024; Longhi et al. 2024). Consequently,

the occurrence of several dated failures near the beginning of the Holocene might not by itself be regarded as evidence for an Alpine-wide phase of synchronous climate-triggered instability.

The most plausible interpretation is that the Poschiavo source slope was progressively preconditioned by glacial valley erosion, repeated loading and unloading, geological structure and long-term fracture development (Grämiger et al. 2017). Environmental changes at the beginning of the Holocene may have contributed to final destabilization through thermal or hydrological effects, while seismic shaking represents an alternative short-lived trigger. None of these mechanisms can presently be demonstrated independently. Detailed structural and geomechanical mapping of the source area, together with more precise regional palaeoseismic and palaeohydrological records, would be required to distinguish among them. The present study therefore constrains the age and environmental context of the Poschiavo event, but its immediate trigger remains unresolved.

Conclusion

This study combines geomorphological mapping, petrographic observations, cosmogenic ^{10}Be exposure dating, palaeotopographic reconstruction, volume estimation, and DAN3D® runout modelling to investigate the origin, timing, and emplacement of the Mota dal Meschin deposit in the Poschiavo Valley. The mapped body is interpreted as a single rock avalanche deposit, rather than as either a glacial deposit or a rock avalanche deposit subsequently overridden by glacier ice and covered by till. The irregular surface morphology, abundance of large angular boulders, locally preserved openwork fabric support this interpretation. No till cover was identified, and the exposed sections show no evidence of substantial post-emplacement glacial overriding.

Nine ^{10}Be exposure ages define a statistically coherent age population with a mean age of 11.1 ± 0.5 ka. The agreement between samples from the main Mota dal Meschin deposit and the Garbella ridge indicates that these surfaces were exposed during one principal catastrophic event. Although minor inheritance, post-depositional modification, or additional failures preserved only in the subsurface cannot be excluded, the chronology provides the best available age estimate for emplacement of the preserved surface deposit. The event therefore occurred in the Early Holocene, shortly after the Younger Dryas-Holocene transition.

Petrographic similarities between the boulders and crystalline bedrock of the Bernina Nappe confirm a local source, but do not independently distinguish between the two valley flanks. The combined topographic, volumetric, geomorphological, and modelling evidence favours a release area on the southwestern flank between Giümelin and Corn dal Solcun. The present deposit volume is estimated at approximately 94 Mm^3, corresponding to an intact source volume of approximately 76 Mm^3 when a 20% bulking factor is assumed. These values remain first order estimates

because the original source morphology, buried valley-floor topography, and extent of eroded or concealed deposits are incompletely constrained.

The best-fit DAN3D® simulations show that a single large failure could reproduce the first-order distribution of the mapped deposits. The simulated mass reached the valley floor within approximately 50 s, spread across the overdeepened basin, and came to rest after about 6–8 min. The mapped bodies at Mota dal Meschin, La Motina, and Li Plani are therefore interpreted as remnants of a formerly more continuous deposit that was subsequently fragmented by incision of the Poschiavino River and partly buried by debris-flow and alluvial-fan deposition. The rock avalanche probably obstructed the valley and influenced the subsequent development of Lake Poschiavo, although the original dam geometry, former lake levels, and relationship to any pre-existing lake remain unresolved.

The main Poschiavo Valley was most likely ice-free at the time of failure, making active glacier retreat at Miralago an unlikely immediate trigger. Earlier glaciations nevertheless likely preconditioned the source slope through valley overdeepening, slope steepening, unloading, and progressive rock mass damage. Climatic and hydrological changes at the beginning of the Holocene and regional seismic shaking remain plausible final triggers, but neither can be demonstrated directly from the available evidence.

Overall, the study identifies the Mota dal Meschin deposit as the product of a major Early Holocene rock avalanche, constrains its age and probable source area, and provides a mechanically plausible reconstruction of its emplacement. It also illustrates how large rock avalanche deposits in formerly glaciated valleys may be misidentified as glacial sediments and subsequently obscured by younger landscape processes. Further structural mapping of the source area, geophysical investigation of the lake basin, and direct dating of buried mass-movement units would be required to resolve the full event history, lake evolution, and immediate trigger.

Acknowledgments

Special thanks go to Julijana Gajic for her assistance with laboratory introduction and sample preparation at the Institute of Geological Sciences, University of Bern. We would like to extend our gratitude to Marius Schneider for his support and assistance during the modelling process. We also thank the Zürich AMS Facility operated by the Swiss Federal Institute of Technology (ETH Zürich) for conducting the AMS analyses.

Additional information

Conflict of interest

The authors have declared that no competing interests exist.

Ethical statement

No ethical statement was reported.

Use of AI

Artificial intelligence (AI) assistance was used exclusively for language editing and improving the clarity of the manuscript.

Funding

This study is funded by the Glacial Geology Group at the Institute of Geological Sciences, University of Bern. We are thankful for the financial support from CH-Quat for the fieldwork.

Author contributions

Conceptualization: JA, NA, SIO. Data curation: JF, MC, PG. Formal analysis: SIO, JA, JF. Funding acquisition: NA. Investigation: JF. Methodology: NA, SIO, JA. Project administration: NA. Software: JA. Supervision: DM, JA, NA, SIO. Validation: SIO, JA. Visualization: JF. Writing – original draft: JF, DM, SIO, NA, JA, PG, MC. Writing - review and editing: JF, DM, SIO, NA, JA, PG, MC

Author ORCIDs

Naki Akçar https://orcid.org/0000-0002-5604-3179

Jordan Aaron https://orcid.org/0000-0001-8414-106X

David Mair https://orcid.org/0000-0002-7018-6416

Susan Ivy-Ochs https://orcid.org/0000-0002-3242-9536

Data Resources

We provide all of the Data that support the findings of this study in the main text.

References

Aaron J, McDougall S, Kowalski J, Mitchell A, Nolde N (2022) Probabilistic prediction of rock avalanche runout using a numerical model. Landslides 19: 2853–2869. https://doi.org/10.1007/s10346-022-01939-y

Abbühl LM, Akçar N, Strasky S, Graf AA, Ivy-Ochs S, Schlüchter C (2009) A zero-exposure time test on an erratic boulder: evaluating the problem of pre-exposure in surface exposure dating. E&G Quaternary Science Journal 58(1): 1–11. https://doi.org/10.3285/eg.58.1.01

Abele G (1974) Bergstürze in den Alpen: ihre Verbreitung, Morphologie und Folgeerscheinungen. Wissenschaftliche Alpenvereinshefte 25. Deutscher Alpenverein, Munich, 230 pp.

Akçar N, Ivy-Ochs S, Kubik PW, Schlüchter C (2011) Post-depositional impacts on 'Findlinge' (erratic boulders) and their implications for Surface exposure dating.

Swiss Journal of Geosciences 104(3): 445–453. https://doi.org/10.1007/s00015-011-0088-7

Akçar N, Ivy-Ochs S, Deline P, Alfimov V, Kubik PW, Christl M, Schlüchter C (2014) Minor inheritance inhibits the calibration of the 10 Be production rate from the AD 1717 Val Ferret rock avalanche, European Alps. Journal of Quaternary Science 29(4): 318–328. https://doi.org/10.1002/jqs.2706

Akçar N, Deline P, Ivy-Ochs S, Alfimov V, Hajdas I, Kubik PW, Christl M, Schlüchter C (2012) The AD 1717 rock avalanche deposits in the upper Ferret Valley, Italy: a dating approach with cosmogenic 10Be. Journal of Quaternary Science 27(4): 383–392. https://doi.org/10.1002/jqs.1558

Akçar N, Ivy-Ochs S, Alfimov V, Schlunegger F, Claude A, Reber R, Christl M, Vockenhuber C, Dehnert A, Rahn M, Schlüchter C (2017) Isochron-burial dating of glaciofluvial deposits: First results from the Swiss Alps. Earth Surface Processes and Landforms 42(14): 2414–2425. https://doi.org/10.1002/ESP.4201

Aksay S, Ivy-ochs S, Hippe K, Grämiger L, Vockenhuber C (2021) Slope Failure in a Period of Increased Landslide Activity: Sennwald Rock Avalanche, Switzerland. Geosciences 2021, Vol. 11, Page 331 11: 331. https://doi.org/10.3390/GEOSCIENCES11080331

André MF (2002) Rates of postglacial rock weathering on glacially scoured outcrops (abisko–riksgränsen area, 68°n). Geografiska Annaler: Series A, Physical Geography 84: 139–150. https://doi.org/10.1111/J.0435-3676.2002.00168.X

Balco G (2011) Contributions and unrealized potential contributions of cosmogenic-nuclide exposure dating to glacier chronology, 1990–2010. Quaternary Science Reviews, 30(1–2), 3–27. https://doi.org/10.1016/j.quascirev.2010.11.003

Balco G, Stone JO, Lifton NA, Dunai TJ (2008) A complete and easily accessible means of calculating surface exposure ages or erosion rates from 10Be and 26Al measurements. Quaternary Geochronology 3(3): 174–195. https://doi.org/10.1016/J.QUAGEO.2007.12.001

Ballantyne CK (2002) Paraglacial geomorphology. Quaternary Science Reviews, 21(18–19), 1935–2017. https://doi.org/10.1016/S0277-3791(02)00005-7

Ballantyne CK, Sandeman GF, Stone JO, Wilson P (2014) Rock-slope failure following Late Pleistocene deglaciation on tectonically stable mountainous terrain. Quaternary Science Reviews 86: 144–157. https://doi.org/10.1016/j.quascirev.2013.12.021

Bellwald B, Nigg V, Fabbri SC, Becker LWM, Gilli A, Anselmetti FS (2024) Holocene seismic activity in south-eastern Switzerland: evidence from the sedimentary record of Lake Silvaplana. Sedimentology 71(1): 116–151. https://doi.org/10.1111/sed.13131

Bichler MG, Reindl M, Reitner JM, Drescher-Schneider R, Wirsig C, Christl M, Hajdas I, Ivy-Ochs S (2016) Landslide deposits as stratigraphical markers for a sequence-based glacial stratigraphy: a case study of a Younger Dryas system in the Eastern Alps. Boreas 45(3): 537–551. https://doi.org/10.1111/BOR.12173

Bini A, Buoncristiani JF, Couterrand S, Ellwanger D, Felber M, Florineth D, Graf HR, Keller O, Kelly M, Schlüchter C, Schoeneich P (2009) Switzerland during the Last Glacial Maximum (LGM), 1:500 000. Federal Office of Topography Swisstopo, Wabern. [Map.]

Borgatti L, Soldati M (2010) Landslides as a geomorphological proxy for climate change: A record from the Dolomites (northern Italy). Geomorphology, 120(1–2), 56–64. https://doi.org/10.1016/J.GEOMORPH.2009.09.015

Breitenmoser T, Thöny R, Figi D (2022) Geologisch-hydrogeologische Detailuntersuchungen. Schweizerische Zeitschrift für Forstwesen 173(3): 130–136. https://doi.org/10.3188/szf.2022.0130

Brückl E, Parotidis M (2005) Prediction of slope instabilities due to deep-seated gravitational creep. Natural Hazards and Earth System Sciences 5: 155–172. https://doi.org/10.5194/nhess-5-155-2005

Bucher G, Dieleman C, Ivy-Ochs S, Aaron J, Vockenhuber C, Akçar N (2024) Deciphering the dynamics of a Younger Dryas rock avalanche in the Bernese Alps. Swiss Journal of Geosciences, 117(1). https://doi.org/10.1186/S00015-024-00470-7

Burga CA (1987) Gletscher- und Vegetationsgeschichte der südrätischen Alpen seit der Späteiszeit: Puschlav, Livigno, Bormiese. Denkschriften der Schweizerischen Naturforschenden Gesellschaft 101. Basel: Birkhäuser

Chmeleff J, von Blanckenburg F, Kossert K, Jakob D (2010) Determination of the 10Be half-life by multicollector ICP-MS and liquid scintillation counting. Nuclear Instruments and Methods in Physics Research Section B: Beam Interactions with Materials and Atoms 268: 192–199. https://doi.org/10.1016/J.NIMB.2009.09.012

Christl M, Vockenhuber C, Kubik PW, Wacker L, Lachner J, Alfimov V, Synal HA (2013) The ETH Zurich AMS facilities: Performance parameters and reference materials. Nuclear Instruments and Methods in Physics Research Section B: Beam Interactions with Materials and Atoms 294: 29–38. https://doi.org/10.1016/J.NIMB.2012.03.004

Church M, Ryder JM (1972) Paraglacial sedimentation: a consideration of fluvial processes conditioned by glaciation. Geological Society of America Bulletin 83(10): 3059–3072. https://doi.org/10.1130/0016-7606(1972)83[3059:PSACOF]2.0.CO;2

Conrad O (2009) SAGA-GIS Tool Library Documentation (v3.0.0). https://saga-gis.sourceforge.io/saga_tool_doc/3.0.0/imagery_vigra_0.html

Cook SJ, Porter PR, Bendall CA (2013) Geomorphological consequences of a glacier advance across a paraglacial rock avalanche deposit. Geomorphology 189: 109–120. https://doi.org/10.1016/j.geomorph.2013.01.022

Costa JE, Schuster RL (1988) The formation and failure of natural dams. Geological Society of America Bulletin 100: 1054–1068. https://doi.org/10.1130/0016-7606(1988)100%3C1054:TFAFON%3E2.3.CO;2

De Palézieux L, Loew S (2019) Long-term transient groundwater pressure and deep infiltration in Alpine mountain slopes (Poschiavo Valley, Switzerland). Hydrogeology Journal 27: 2817–2834. https://doi.org/10.1007/S10040-019-02025-9

Deline P, Akçar N, Ivy-Ochs S, Kubik PW (2015) Repeated Holocene rock avalanches onto the Brenva Glacier, Mont Blanc massif, Italy: a chronology. Quaternary Science Reviews 126: 186–200. https://doi.org/10.1016/j.quascirev.2015.09.004

Deline P, Kirkbride MP (2009) Rock avalanches on a glacier and morainic complex in Haut Val Ferret, Mont Blanc Massif, Italy. Geomorphology 103(1): 80–92. https://doi.org/10.1016/j.geomorph.2007.10.020

Deplazes G, Anselmetti FS, Hajdas I (2007) Lake sediments deposited on the Flims rockslide mass: the key to date the largest mass movement of the Alps. Terra Nova, 19(4), 252-258. https://doi.org/10.1111/j.1365-3121.2007.00743.x

Dieleman C, Deline P, Ivy-Ochs S, Hug P, Aaron J, Christl M, Akçar N (2025) Unravelling the evolution of the Frébouge polygenetic cone in Val Ferret (Mont Blanc Massif). Boreas, e70042. https://doi.org/10.1111/bor.70042.

Dortch JM, Tomkins MD, Saha S, Murari MK, Schoenbohm LM, Curl D (2022) A tool for the ages: The Probabilistic Cosmogenic Age Analysis Tool (P-CAAT). Quaternary Geochronology 71: 101323. https://doi.org/10.1016/j.quageo.2022.101323

Fan X, Scaringi G, Korup O, West AJ, van Westen CJ, Tanyas H, Hovius N, Hales TC, Jibson RW, Allstadt KE, Zhang L, Evans SG, Xu C, Li G, Pei X, Xu Q, Huang R (2019) Earthquake-induced chains of geologic hazards: Patterns, mechanisms, and impacts. Reviews of Geophysics 57(2): 421–503. https://doi.org/10.1029/2018RG000626

Federal office of Topography Swisstopo (2023) SwissAlti3D dataset 0.5m. https://www.swisstopo.admin.ch/en/height-model-swissalti3d

Federal office of Topography Swisstopo (2024) Tectonic Map of Switzerland 1:500 000 TK500. https://www.swisstopo.admin.ch/en/geomaps-500-vector

Federal office of Topography Swisstopo (2026) Mapsheet LK1298 Geocover dataset 1:25’000. https://www.swisstopo.admin.ch/en/geological-model-2d-geocover

Fischer L, Purves RS, Huggel C, Noetzli J, Haeberli W (2012) On the influence of topographic, geological and cryospheric factors on rock avalanches and rockfalls in high-mountain areas. Natural Hazards and Earth System Sciences 12: 241–254. https://doi.org/10.5194/nhess-12-241-2012

Gallach X, Ravanel L, Egli M, Brandová D, Schaepman ME, Christl M, Gruber S, Deline P, Carcaillet J, Pallandre F (2018) Timing of rockfalls in the Mont Blanc massif (Western Alps): evidence from Surface exposure dating with cosmogenic 10Be. Landslides 15: 1991–2000. https://doi.org/10.1007/s10346-018-0999-8

Gischig VS, Moore JR., Evans KF, Amann F, Loew S (2011a) Thermomechanical forcing of deep rock-slope deformation: 1. Conceptual study of a simplified slope.

Journal of Geophysical Research: Earth Surface, 116: F04010. https://doi.org/10.1029/2011JF002006.

Gischig VS, Moore JR., Evans KF, Amann F, Loew S (2011b) Thermomechanical forcing of deep rock-slope deformation: 2. The Randa rock-slope instability. Journal of Geophysical Research: Earth Surface, 116: F04011. https://doi.org/10.1029/2011JF002007

Gosse JC, Phillips FM (2001) Terrestrial in situ cosmogenic nuclides: theory and application. Quaternary Science Reviews 20(14): 1475–1560. https://doi.org/10.1016/S0277-3791(00)00171-2

Gouffon Y (editor) (2024) Tectonic Map of Switzerland 1:500 000: Explanatory notes. Federal Office of Topography swisstopo, Wabern, 155 pp. ISBN 978-3-302-40125-6

Grämiger LM, Moore JR, Gischig VS, Loew S (2018) Thermomechanical stresses drive damage of Alpine valley rock walls during repeat glacial cycles. Journal of Geophysical Research: Earth Surface 123(10): 2620–2646. https://doi.org/10.1029/2018JF004626

Grämiger LM, Moore JR, Gischig VS, Ivy-Ochs S, Loew S (2017) Beyond debuttressing: mechanics of paraglacial rock-slope damage during repeat glacial cycles. Journal of Geophysical Research: Earth Surface 122(4): 1004–1036. https://doi.org/10.1002/2016JF003967

Grämiger LM, Moore JR, Vockenhuber C, Aaron J, Hajdas I, Ivy-Ochs S (2016) Two Early Holocene rock avalanches in the Bernese Alps (Rinderhorn, Switzerland). Geomorphology 268: 207–221. https://doi.org/10.1016/j.geomorph.2016.06.008

Grämiger LM, Moore JR, Gischig VS, Loew S, Funk M, Limpach P (2020) Hydromechanical rock-slope damage during Late Pleistocene and Holocene glacial cycles in an Alpine valley. Journal of Geophysical Research: Earth Surface 125(8): e2019JF005494. https://doi.org/10.1029/2019JF005494

Gruber S, Haeberli W (2007) Permafrost in steep bedrock slopes and its temperature-related destabilization following climate change. Journal of Geophysical Research: Earth Surface 112: F02S18. https://doi.org/10.1029/2006JF000547

Gunzburger Y, Merrien-Soukatchoff V, Guglielmi Y (2005) Influence of daily surface temperature fluctuations on rock slope stability: case study of the Rochers de Valabres slope (France). International Journal of Rock Mechanics and Mining Sciences 42(3): 331–349. https://doi.org/10.1016/J.IJRMMS.2004.11.003

Hainzl S, Kraft T, Wassermann J, Igel H, Schmedes E (2006) Evidence for rainfall-triggered earthquake activity. Geophysical Research Letters, 33(19). https://doi.org/10.1029/2006GL027642

Hartmeyer I, Delleske R, Keuschnig M, Krautblatter M, Lang A, Christoph Otto J, Schrott L (2020) Current glacier recession causes significant rockfall increase: The immediate paraglacial response of deglaciating cirque walls. Earth Surface Dynamics 8: 729–751. https://doi.org/10.5194/ESURF-8-729-2020

Heyman J, Stroeven AP, Harbor JM, Caffee MW (2011) Too young or too old: evaluating cosmogenic exposure dating based on an analysis of compiled boulder exposure ages. Earth and Planetary Science Letters, 302(1–2), 71–80. https://doi.org/10.1016/j.epsl.2010.11.040

Heyman J, Applegate PJ, Blomdin R, Gribenski N, Harbor JM, Stroeven AP (2016) Boulder height–exposure age relationships from a global glacial 10Be compilation. Quaternary Geochronology 34: 1–11. https://doi.org/10.1016/j.quageo.2016.03.002

Hilger P, Gosse JC, Hermanns RL (2019) How significant is inheritance when dating rockslide boulders with terrestrial cosmogenic nuclide dating?—A case study of an historic event. Landslides 16(4): 729–738. https://doi.org/10.1007/s10346-018-01132-0

Hormes A, Ivy-Ochs S, Kubik PW, Ferreli L, Maria Michetti A (2008) 10Be exposure ages of a rock avalanche and a late glacial moraine in Alta Valtellina, Italian Alps. Quaternary International 190(1): 136–145. https://doi.org/10.1016/J.QUAINT.2007.06.036

Hungr O, Evans SG (2004) Entrainment of debris in rock avalanches: An analysis of a long run-out mechanism. GSA Bulletin, 116(9–10): 1240–1252. https://doi.org/10.1130/B25362.1

Hungr O, McDougall S (2009) Two numerical models for landslide dynamic analysis. Computers & Geosciences 35(5): 978–992. https://doi.org/10.1016/j.cageo.2007.12.003

Ivy-Ochs S, Kober F (2008) Surface exposure dating with cosmogenic nuclides. E&G Quaternary Science Journal, 57(1/2): 179–209. https://doi.org/10.3285/EG.57.1-2.7

Ivy-Ochs S, Monegato G, Reitner JM (2022) The Alps: Glacial landforms from the Last Glacial Maximum. In D. Palacios, P.D. Hughes, J.M. García-Ruiz, and N. Andrés (eds), European Glacial Landscapes: Maximum Extent of Glaciations, 449–460. Elsevier. https://doi.org/10.1016/B978-0-12-823498-3.00030-3.

Ivy-Ochs S, Monegato G, Reitner JM (2023a) Chapter 20 - The Alps: glacial landforms during the deglaciation (18.9–14.6 ka). In: Palacios D, Hughes PD, García-Ruiz JM, Andrés N (Eds) European Glacial Landscapes. Elsevier, 175–183. https://doi.org/10.1016/B9780-323-91899-2.00005-X

Ivy-Ochs S, Monegato G, Reitner JM (2023b) Chapter 55 - The Alps: glacial landforms from the Younger Dryas Stadial. In: Palacios D, Hughes PD, García-Ruiz JM, Andrés N (Eds) European Glacial Landscapes. Elsevier, 525–539. https://doi.org/10.1016/B978-0323-91899-2.00058-9

Ivy-Ochs S, Kerschner H, Kubik PW, Schlüchter C (2006) Glacier response in the European Alps to Heinrich Event 1 cooling: The Gschnitz stadial. Journal of Quaternary Science 21(2): 115–130. https://doi.org/10.1002/JQS.955

Ivy-Ochs S, von Poschinger A, Synal HA, Maisch M (2009a) Surface exposure dating of the Flims landslide, Graubünden, Switzerland. Geomorphology 103(1): 104–112. https://doi.org/10.1016/J.GEOMORPH.2007.10.024

Ivy-Ochs S, Kerschner H, Maisch M, Christl M, Kubik PW, Schlüchter C (2009b) Latest Pleistocene and Holocene glacier variations in the European Alps. Quaternary Science Reviews, 28(21–22), 2137–2149. https://doi.org/10.1016/J.QUASCIREV.2009.03.009

Ivy-Ochs S, Martin S, Campedel P, Hippe K, Alfimov V, Vockenhuber C, Andreotti E, Carugati G, Pasqual D, Rigo M, Viganò A (2017) Geomorphology and age of the Marocche di Dro rock avalanches (Trentino, Italy). Quaternary Science Reviews, 169, pp.188-205. https://doi.org/10.1016/j.quascirev.2017.05.014

Jacquemart M, Weber S, Chiarle M, Chmiel M, Cicoira A, Corona C, Eckert N, Gaume J, Giacona F, Hirschberg J, Kaitna R, Magnin F, Mayer S, Moos C, van Herwijnen A, Stoffel M (2024) Detecting the impact of climate change on alpine mass movements in observational records from the European Alps. Earth-Science Reviews 258: 104886. https://doi.org/10.1016/J.EARSCIREV.2024.104886

Keefer DK (1984) Landslides caused by earthquakes. Geological Society of America Bulletin, 95(4), 406–421. https://doi.org/10.1130/0016-7606(1984)95%3C406:LCBE%3E2.0.CO;2

Kerschner H, Ivy-Ochs S (2008) Palaeoclimate from glaciers: Examples from the Eastern Alps during the Alpine Lateglacial and Early Holocene. Global and Planetary Change, 60(1–2), 58–71. https://doi.org/10.1016/J.GLOPLACHA.2006.07.034

Koltai G, Spötl C, Jarosch AH, Cheng H (2021) Cryogenic cave carbonates in the dolomites (northern Italy): Insights into Younger Dryas cooling and seasonal precipitation. Climate of the Past 17(2): 775–789. https://doi.org/10.5194/CP-17-775-2021

Korschinek G, Bergmaier A, Faestermann T, Gerstmann UC, Knie K, Rugel G, Wallner A, Dillmann I, Dollinger G, von Gostomski CL, Kossert K, Maiti M, Poutivtsev M, Remmert A (2010) A new value for the half-life of 10Be by Heavy-Ion Elastic Recoil Detection and liquid scintillation counting. Nuclear Instruments and Methods in Physics Research Section B: Beam Interactions with Materials and Atoms 268: 187–191. https://doi.org/10.1016/J.NIMB.2009.09.020

Köpfli P, Grämiger LM, Moore JR, Vockenhuber C, Ivy-Ochs S (2018) The Oeschinensee rock avalanche, Bernese Alps, Switzerland: a co-seismic failure 2300 years ago? Swiss Journal of Geosciences, 111, 205–219. https://doi.org/10.1007/s00015-017-0293-0

Kotlarski S, Gobiet A, Morin S, Olefs M, Rajczak J, Samacoïts R (2023) 21st century alpine climate change. Climate Dynamics 60: 65–86. https://doi.org/10.1007/s00382-022-06303-3

Krautblatter M, Funk D, Günzel FK (2013) Why permafrost rocks become unstable: A rock–ice-mechanical model in time and space. Earth Surface Processes and Landforms 38(8): 876–887. https://doi.org/10.1002/esp.3374

Lal D (1991) Cosmic ray labeling of erosion surfaces: in situ nuclide production rates and erosion models. Earth and Planetary Science Letters, 104(2–4), 424–439. https://doi.org/10.1016/0012-821X(91)90220-C

Leith K, Moore JR, Amann F, and Loew S (2014a). Subglacial extensional fracture development and implications for Alpine valley evolution. Journal of Geophysical Research: Earth Surface, 119(1), 62–81. https://doi.org/10.1002/2012JF002691

Leith K, Moore JR, Amann F, and Loew S (2014b). In situ stress control on microcrack generation and macroscopic extensional fracture in exhuming bedrock. Journal of Geophysical Research: Solid Earth, 119(1), 594–615. https://doi.org/10.1002/2012JB009801

Lifton N (2016) Implications of two Holocene time-dependent geomagnetic models for cosmogenic nuclide production rate scaling. Earth and Planetary Science Letters 433: 257–268. https://doi.org/10.1016/J.EPSL.2015.11.006

Le Roy M, Ivy-Ochs S, Nicolussi K, Monegato G, Reitner JM, Colucci RR, Ribolini A, Spagnolo M, Stoffel M (2026) Holocene glacier variations in the Alps. European Glacial Landscapes: The Holocene: 367–418. https://doi.org/10.1016/B978-0-323-99712-6.00018-0

Longhi A, Morgan D, Guglielmin M (2024) Reconstruction of rock avalanche history in Val Viola (Upper Valtellina, Italian Central Alps) through 10Be exposure ages, Schmidt-hammer R-values, and surface roughness. Landslides 21: 949–962. https://doi.org/10.1007/s10346-024-02210-2

Manconi A, Jones N, Loew S, Strozzi T, Caduff R, Wegmueller U (2024) Monitoring surface deformation with spaceborne radar interferometry in landslide complexes: insights from the Brienz/Brinzauls slope instability, Swiss Alps. Landslides 21(10): 2519–2533. https://doi.org/10.1007/S10346-024-02291-Z

Maxeiner S, Synal HA, Christl M, Suter M, Müller A, Vockenhuber C (2019) Proof-of-principle of a compact 300 kV multi-isotope AMS facility. Nuclear Instruments and Methods in Physics Research Section B: Beam Interactions with Materials and Atoms 439: 84–89. https://doi.org/10.1016/J.NIMB.2018.11.028

McColl ST (2012) Paraglacial rock-slope stability. Geomorphology, 153–154, 1–16. https://doi.org/10.1016/j.geomorph.2012.02.015

McColl ST (2020) The anomalously old Bush Stream rock avalanche and its implications for landslide inventories in dynamic landscapes. Frontiers in Earth Science 8: 103. https://doi.org/10.3389/feart.2020.00103

McColl ST, Davies TRH (2013) Large ice-contact slope movements: glacial buttressing, deformation and erosion. Earth Surface Processes and Landforms 38(10): 1102–1115. https://doi.org/10.1002/esp.3346

McColl ST, Draebing D (2019) Rock-slope instability in the proglacial zone: state of the art. In T. Heckmann and D. Morche (eds), Geomorphology of Proglacial Systems: Landform and Sediment Dynamics in Recently Deglaciated Alpine Landscapes, pp. 119–141. Springer, Cham. https://doi.org/10.1007/978-3-319-94184-4_8

McDougall S (2017) 2014 Canadian geotechnical colloquium: Landslide runout analysis — current practice and challenges. Canadian Geotechnical Journal 54(5): 605–620. https://doi.org/10.1139/cgj-2016-0104

McDougall S, Hungr E (2004) A model for the analysis of rapid landslide motion across three-dimensional terrain. Canadian Geotechnical Journal 41(6): 1084-1097. https://doi.org/10.1139/t04-052

Neteler M, Bowman MH, Landa M, Metz M (2012) GRASS GIS: A multi-purpose open source GIS. Environmental Modelling & Software 31: 124–130. https://doi.org/10.1016/J.ENVSOFT.2011.11.014

Nicolussi K, Spötl C, Thurner A, Reimer PJ (2015) Precise radiocarbon dating of the giant Köfels landslide (Eastern Alps, Austria). Geomorphology 243: 87–91. https://doi.org/10.1016/j.geomorph.2015.05.001

Nicolussi K, Le Roy M, Hajdas I, Pichler T, Wacker L, Schlüchter C (2026) Chasing the melting ice: evidence for the earliest Holocene glacier minimum in the Alps and precise dating of the subsequent advance at the end of the Preboreal. Quaternary Science Reviews 388: 109962. https://doi.org/10.1016/J.QUASCIREV.2026.109962

Nie W, Krautblatter M, Leith K, Thuro K, Festl J (2017) A modified tank model including snowmelt and infiltration time lags for deep-seated landslides in alpine environments (Aggenalm, Germany). Natural Hazards and Earth System Sciences 17: 1595–1610. https://doi.org/10.5194/nhess-17-1595-2017

Ostermann M, Sanders D, Ivy-Ochs S, Alfimov V, Rockenschaub M, Römer A (2012) Early Holocene (8.6 ka) rock avalanche deposits, Obernberg Valley, Eastern Alps: landform interpretation and kinematics of rapid mass movement. Geomorphology, 171–172, 83–93. https://doi.org/10.1016/j.geomorph.2012.05.006.

Pánek T (2019) Landslides and Quaternary climate changes—the state of the art. Earth-Science Reviews 196: 102871. https://doi.org/10.1016/j.earscirev.2019.05.015

Paranunzio R, Laio F, Chiarle M, Nigrelli G, Guzzetti F (2016) Climate anomalies associated with the occurrence of rockfalls at high elevation in the Italian Alps. Natural Hazards and Earth System Sciences 16: 2085–2106. https://doi.org/10.5194/nhess-16-2085-2016

Patton AI, Rathburn SL, Capps DM, McGrath D, Brown RA (2021) Ongoing Landslide Deformation in Thawing Permafrost. Geophysical Research Letters 48(16): e2021GL092959. https://doi.org/10.1029/2021GL092959

Pfiffner OA (2022) The Flims rock avalanche: structure and consequences. Swiss Journal of Geosciences 115(24). https://doi.org/10.1186/s00015-022-00424-x

Pfiffner OA, Ivy-Ochs S, Mussina Z, Aaron J, Steinemann O, Vockenhuber C, Akçar N (2023) The Tamins rock avalanche (eastern Switzerland): timing and emplacement processes. Landslides 20(5): 877–899. https://doi.org/10.1007/S10346-022-02004-4

Porter SC, Orombelli G (1980) Catastrophic rockfall of September 12, 1717 on the Italian flank of the Mont Blanc Massif. Zeitschrift für Geomorphologie, Neue Folge, 24, 200–218. https://doi.org/10.1127/zfg/24/1984/200

Prager C, Zangerl C, Patzelt G, Brandner R (2008) Age distribution of fossil landslides in the Tyrol (Austria) and its surrounding areas. Natural Hazards and Earth System Science 8(2): 377–407. https://doi.org/10.5194/NHESS-8-377-2008

Preusser F, Reitner JM, Schlüchter C (2010) Distribution, geometry, age and origin of overdeepened valleys and basins in the Alps and their foreland. Swiss Journal of Geosciences 103: 407–426. https://doi.org/10.1007/S00015-010-0044-Y/FIGURES/11

Reynard E, Häuselmann P, Jeannin PY, Scapozza C (2021) Geomorphological Landscapes in Switzerland. In: Reynard, E. (eds) Landscapes and Landforms of Switzerland. World Geomorphological Landscapes, 71–80. Springer, Cham. https://doi.org/10.1007/978-3-030-43203-4_5

Rubin A, Akçar N, Ivy-Ochs S, Binaghi M, Aaron J, Vockenhuber C, Schlüchter C (2026) The Sierre landslide: chronology, dynamics, and insights into Alpine post-glacial instabilities. Swiss Journal of Geosciences 119: 5-32 119: 5–32. https://doi.org/10.3897/SJG.119.180346

Schaefer JM, Codilean AT, Willenbring JK, Lu ZT, Keisling B, Fülöp RH, Val P (2022) Cosmogenic nuclide techniques. Nature Reviews Methods Primers 2022 2:1 2: 18-. https://doi.org/10.1038/s43586-022-00096-9

Schindelwig I, Akçar N, Kubik PW, Schlüchter C (2012) Lateglacial and Early Holocene dynamics of adjacent valley glaciers in the Western Swiss Alps. Journal of Quaternary Science 27(1): 114–124. https://doi.org/10.1002/jqs.1523

Schleier M, Hermanns RL, Rohn J, Gosse JC (2015) Diagnostic characteristics and paleodynamics of supraglacial rock avalanches, Innerdalen, Western Norway. Geomorphology 245: 23–39. https://doi.org/10.1016/j.geomorph.2015.04.033

Schlüchter C, Akçar N, Ivy-Ochs S (2021) The Quaternary Period in Switzerland. In E. Reynard (ed.), Landscapes and Landforms of Switzerland, 47–69. Cham: Springer. https://doi.org/10.1007/978-3-030-43203-4_4

Seguinot J, Delaney I (2021) Last-glacial-cycle glacier erosion potential in the Alps. Earth Surface Dynamics 9: 923–935. https://doi.org/10.5194/esurf-9-923-2021

Shugar DH, Clague JJ (2011) The sedimentology and geomorphology of rock avalanche deposits on glaciers. Sedimentology 58(7): 1762–1783. https://doi.org/10.1111/j.1365-3091.2011.01238.x

Singeisen C, Ivy-Ochs S, Wolter A, Steinemann O, Akçar N, Yeşilyurt S, Vockenhuber C (2020) The Kandersteg rock avalanche (Switzerland): Integrated analysis of a late Holocene catastrophic event. Landslides 17: 1297–1317. https://doi.org/10.1007/s10346-020-01365-y

Spillmann P (1993) Die Geologie des penninisch-ostalpinen Grenzbereichs im südlichen Berninagebirge. PhD Thesis, ETH Zürich, Zürich, Switzerland. https://doi.org/10.3929/ethz-a-000928802

Spreafico MC, Sternai P, Agliardi F (2021) Paraglacial rock-slope deformations: sudden or delayed response? Insights from an integrated numerical modelling approach. Landslides 18: 1311–1326. https://doi.org/10.1007/s10346-020-01560-x

Staub R (1946) Geologische Karte der Bernina-Gruppe und ihrer Umgebung im Oberengadin, Bergell, Val Malenco, Puschlav und Livigno, 1:50 000. Geologische Spezialkarte der Schweiz 118. Schweizerische Geologische Kommission, Bern.

Stead D, Wolter A (2015) A critical review of rock slope failure mechanisms: The importance of structural geology. Journal of Structural Geology 74: 1–23. https://doi.org/10.1016/J.JSG.2015.02.002

Stone JO (2000) Air pressure and cosmogenic isotope production. Journal of Geophysical Research: Solid Earth, 105(B10), 23753–23759. https://doi.org/10.1029/2000JB900181

Swiss Seismological Service SED Earthquakes. Available from: https://www.seismo.ethz.ch/en/earthquakes/switzerland/last-90-days/ (August 23, 2026).

Tikhomirov D, Akçar N, Ivy Ochs S, Alfimov V, Schlüchter C (2014) Calculation of shielding factors for production of cosmogenic nuclides in fault scarps. Quaternary Geochronology 19: 181–193. https://doi.org/10.1016/J.QUAGEO.2013.08.004

Ye S, Cuzzone JK, Marcott SA, Licciardi JM, Ward DJ, Heyman J, Quinn DP (2023) A quantitative assessment of snow shielding effects on surface exposure dating from a western North American 10Be data compilation. Quaternary Geochronology 76: 101440. https://doi.org/10.1016/J.QUAGEO.2023.101440

Zangerl C, Schneeberger A, Steiner G, Mergili M (2021) Geographic-information-system-based topographic reconstruction and geomechanical modelling of the Köfels rockslide. Natural Hazards and Earth System Sciences 21(8): 2461–2483. https://doi.org/10.5194/nhess-21-2461-2021

Zwahlen P (2019) Der Bergsturz von Miralago: Talgeschichte im Valposchiavo. Swiss Bulletin für Angewandte Geologie, 24(1), 69–80. https://doi.org/10.5169/seals-869527